MASSACHUSETTS INSTITUTE
OF TECHNOLOGY
JUN 16 2009
LIBRARIES

Bio-Inspired Fluid Locomotion

by

Brian Chan

Submitted to the Department of Mechanical Engineering
in partial fulfillment of the requirements for the degree of

Doctor of Science in Mechanical Engineering

at the

MASSACHUSETTS INSTITUTE OF TECHNOLOGY

ARCHIVES

June 2009

© Massachusetts Institute of Technology 2009. All rights reserved.

Author ....
Department of Mechanical Engineering
May 7, 2009

Certified by....................................
Anette Hosoi
Professor
Thesis Supervisor

Accepted by ....
David Hardt
Chairman, Committee on Graduate Students

Bio-Inspired Fluid Locomotion

by

Brian Chan

Submitted to the Department of Mechanical Engineering
on May 7, 2009, in partial fulfillment of the
requirements for the degree of
Doctor of Science in Mechanical Engineering

Abstract

We have developed several novel methods of locomotion at low Reynolds number, for both Newtonian and non-Newtonian fluids: Robosnails 1 and 2, which operate on a lubrication layer, and the three-link swimmer which moves in an unbounded fluid. Robosnail 1 utilizes lubrication pressures generated in a Newtonian fluid under a steadily undulating foot to propel itself forward. Tractoring force and velocity measurements are in agreement with analytic and numerical solutions. Robosnail 2, modeled after real land snails, uses in-plane compressions of a flat foot on a mucus substitute such as Laponite or Carbopol. Robosnail 2 exploits the non-Newtonian qualities (yield-stress, shear thinning) of the fluid solution to locomote. The glue-like behavior of the unyielded fluid allows Robosnail 2 to climb up a 90 degree incline or inverted 180 degree surfaces. The three-link swimmer is a device composed of three rigid links interconnected by two out-of-phase oscillating joints. It is the first experimental test that successfully demonstrates that a swimmer of its kind can translate in the Stokes limit.

Thesis Supervisor: Anette Hosoi
Title: Professor

Acknowledgments

The author would like to thank Anette Hosoi for her patience, guidance and encouragement, David Hu and John Bush for their assistance with fluid dynamics experiments, Julio Guerrero for his guidance, encouragement and help with experimental setups, Gareth McKinley for his fluids knowledge, Randy Ewoldt for sharing his work on non-Newtonian fluids, and his parents and brother for their support.

Additional thanks goes to (in no particular order) Amos Winter, Tony Yu, Sungyon Lee, David Hu, Roger Yeh, Sunny Jung, Dawn Wendell, Darren Crowdy, Sarah Bates, Catherine Koveal, Susan Ji, Neil Balmforth, Ed Summers, Mark Belanger, Fred Cote, Christian Clasen, Doug Hart, Leslie Regan, Deborah Blanchard, Jason Ku, Sean Buhrmeister, David Gandy, Nelson Lai, Grace Kim, Jose Bico, Giorgia Bettin, Rajay Kumar, Sally Kwok, Albert Liau, Amy Wibowo, Hsiang-wei Lu, Steve Childress, Michael Shelley, Jun Zhang and many other friends.

This Research has been funded by the National Science Foundation, and Schlumberger SDR, LTD.

Contents

1 Introduction **17**

1.1 Motivations 18

1.2 Snail locomotion 19

1.3 Three-link swimmer 20

2 General Theory **23**

2.1 Locomotion at Low Reynolds Number 23

2.2 Lubrication Flows 24

2.3 Snail Locomotion 24

2.3.1 Shear-thinning fluids 25

3 Robosnail 1 **29**

3.1 Introduction 29

3.2 Theory 29

3.2.1 Underlying physics 29

3.2.2 Various wave shapes 34

3.2.3 Three-dimensional effects for a finite-width snail 38

3.2.4 Power and efficiency 42

3.3 Mechanisms 44

3.4 Experiment 49

3.5 Results and Discussion 50

4 Robosnail 2 **55**

4.1 Introduction 55

4.2 Theory 56

4.2.1 Underlying physics 56
4.2.2 Bingham fluid approximation 63
4.2.3 Motion with slippage 64
4.2.4 Power and Efficiency 66
4.2.5 Safety vs. efficiency 69
4.3 Mechanical Design 69
4.4 Experiment 75
4.5 Results and Discussion 75

5 Three-Link Swimmer **79**
5.1 Introduction 79
5.2 Theory 80
5.3 Mechanical Design 82
5.4 Experiment 82
5.5 Results and Discussion 84

6 Applications **87**
6.1 General Applications 87
6.2 Downhole locomotion 87
6.3 Rigless tool Deployment 88
6.4 Flexible robotics 88

7 Conclusion **91**
7.1 Future work 92

List of Figures

1-1 *Helix aspersa* and *Limax maximus*, two land snails which inspired the construction of Robosnail 2, the wall-climbing adhesive locomotion device. (Slugs are officially classified as snails) 20

1-2 One prototype of robosnail 2, moving in an inverted position on a 1 mm layer of Laponite (A synthetic clay suspension) 21

2-1 Shear-rate ($\dot{\gamma}$) versus shear-stress (τ) curves for various fluids. Robosnail 2 exploits the physical properties of non-Newtonian fluids and theoretically can use any of the fluids shown, except for the Newtonian fluid. The four fluids shown above have simple mathematical representations: For the Newtonian fluid $\tau = \mu\dot{\gamma}$, for the power law fluid $\tau = \mu\dot{\gamma}^n$, for the Bingham fluid $\tau = \tau_y + \mu\dot{\gamma}$, and for the Herschel-Bulkley fluid $\tau = \tau_y + \mu\dot{\gamma}^n$. 26

2-2 Shear-rate versus viscosity curves for various concentrations of Carbopol, a synthetic fluid used for the lubrication layer of Robosnail 2 [21, 22]. Note that for each curve, the viscosity drops several orders of magnitude beyond a certain shear stress. This is the shear-thinning behavior; Newtonian fluids possess a constant viscosity regardless of shear rate. This shear-thinning behavior is a critical property that allows Robosnail and most live snails to move. When approximated as a finite yield-stress fluid, the yield stress can be taken as the point at which the viscosity drops off. (Figure appears courtesy of Randy Ewoldt [21]) 27

3-1 Switching to a moving reference frame to find the flow underneath a self-propelled, peristaltic waving membrane. In the laboratory frame, the foot height is a function of x and t. In the wave frame (a frame of reference following the wave crests) the height is only dependent on x and the flow can be modeled as steady. 32

3-2 (Left) The relationship between dimensionless applied force and snail velocity. As the tractoring load is increased to the stall force, the velocity decreases to zero. The full graph extends past $f < 0$, where increasing the tractoring force beyond the stall force would cause the snail to drift backwards, and $V_s > V_{s,free}$ where a negative (pushing) tractoring force would increase the snail velocity past $V_{s,free}$. 34

3-3 Dimensionless stall force and free velocity for a three different wave shapes: sinusoid, sawtooth, and square. Note that the force is displayed on a log scale. As the amplitude gets larger, with the foot nearly touching the substrate, lubrication pressures increase, and the stall force increases rapidly. While the stall force is similar for the three wave shapes across the given range of amplitudes, there is significant variation in the free velocity ([10]) for differing wave shapes. The square wave performs favorably at low amplitudes, but as the amplitude nears $a = 0.5$, the sharper wave profiles gain an advantage. Note that the model predicts that the sawtooth wave can achieve $\hat{V}_s > \hat{V}_w$. 35

3-4 A "composite" waveform made of two parabolas. By varing the sharpness factor f_s (the relative size of the downturned parabola to the entire wavelength) from near 0 to near 1, we can vary the free velocity as a function of the amplitude. 37

3-5 (Left) Dimensionless velocity as a function of the "sharpness ratio" of the two parabolas composing the wave. $\hat{V}_w$. (Right) Maximum velocity attainable as a function of the sharpness ratio f_s. As the lower parabola becomes less than 30 percent of the total wavelength ($f_s = 0.7$), the snail begins to move at a speed greater than the waving speed 37

3-6 A typical Matlab simulation result of pressure underneath a finite width, periodic waving robosnail 1 foot, with an aspect ratio of $b = W/\lambda = 1.6$ and $a = 0.7$. The simulation itself uses a periodic end conditions in x and is mirrored along the x-z plane. The waving foot generates a pressure similar to the two-dimensional waving robosnail foot near the centerline, but at the edges, the fluid is allowed to leak, and pressure decreases, decreasing the total propulsive force. 39

3-7 Tractoring force, snail velocity, and centerline pressure plot for robosnail 1, comparing a finite width snail with an infinitely wide snail. The finite snail has a waving amplitude a 0.7 times the average fluid film height, and a width W equal to 0.8 times the wavelength λ. The wave shapes for both cases are the same. The finite snail suffers from edge leakage, which degrades the maximum tractoring force and velocities, as well as the efficiency. The centerline pressure serves as a qualitative evaluation of how much propulsive pressure is lost overall in the finite case. 40

3-8 Simulation results showing ratio of tractoring force for a finite-width robosnail compared to the same robosnail 2D analytical result, with sinusoidal wave profile. Note that below $a < 0.1$ the expected force ratio asymptotes to the lowest curve. 41

3-9 Maximum efficiency plot of a 2D robosnail with various wave shapes and over a range of amplitudes. The relative efficiency performance of the three wave shapes is comparable to that of the free velocity (Figure 3-3). 43

3-10 Partially exploded view of Robosnail 1 showing motor/gearbox assembly, rotating helix, slot plates, and membrane. 44

3-11 Side cross-section of the “ring snail” with interchangeable cams 46

3-12 Some interchangeable cams that would allow various wave shapes for the ring-shaped periodic robosnail 1. 47

3-13 Another robosnail 1 type design for generating a non-sinusoidal waveform in the membrane. This particular design aims to test the "overdrive" phenomenon where the snail velocity exceeds its own waveform velocity. The membrane is reinforced with lateral stiffness members, and is stretched across two spiral cams. The rotational motion of the pair of spiral cams would transfer their translating profile to the membrane. 48

3-14 Set-up for measuring free velocity of robosnail. The channel contains the working fluid, enough to submerge the entire foot so that the peristaltic motion does not entrain air bubbles during operation. A laser sheet is shone at an angle onto the bottom foot surface, so that the profile could be measured and the wave profile and fluid thickness determined. 49

3-15 Set-up for measuring the moving tractoring force of the snail. Small support wheels on tracks hold the snail at a fixed height from the substrate, while the pulley setup allows the payload to be easily adjusted. 50

3-16 Free velocity of robosnail plotted against waving velocity. Fluid is silicone oil. The best-fit line coincides with the numerical result for a finite-width snail with dimensionless waving amplitude $a = 0.8$. 51

3-17 Tractoring force of Robosnail 1, plotted against waving velocity. The resultant tractoring force is linearly proportional with respect to waving velocity, as expected. The solid line represents the corresponding tractoring force predicted by numerical results for a snail of aspect ratio $b/l = 0.6$ with a sinusoidal wave amplitude ratio of $a/h = 0.7$. Fluid is silicone oil. 52

3-18 Force-velocity data for Robosnail 1. The payload force was increased while the robosnail velocity was measured. The snail velocity decreased linearly as expected. Fluid is silicone oil. The foot aspect ratio is aspect ratio $b/l = 0.6$, with a sinusoidal wave amplitude ratio of $a/h = 0.7$. 53

4-1 The underside of a moving slug (*Limax maximus*). The foot is divided into several regions; the interwave, which has material points stationary with respect to the glass surface, the waves, which are sliding forward with respect to the glass, and the rim, which is sliding at a constant velocity with respect to the glass. This study will focus on the wave and interwave regions. . . . 57

4-2 Snails moving with adhesive locomotion may apply direct or retrograde waves. The vertical stripes represent the relative local compression of the foot surface. Direct waves are necessarily waves of compression, while retrograde waves are necessarily waves of expansion 58

4-3 A space-time representation of the waves and interwaves of the foot of a moving snail (from [10]). As the waves and interwaves move forward at a given velocity, the actual material points of the foot (given by the dotted line) move at a different velocity: while the point is within the interwave, it is stationary even though the interwave moves forward; while the point is within the wave, it moves faster than the velocity of the wave zones. L_W and L_I are the wave velocities, respectively, and $\hat{t}_w$ $\hat{t}_i$ are the times a material point remains within a wave and interwave, respectively. $\hat{X}_W$ is the increment of distance that the snail travels during the passage of a single wave. 58

4-4 The motion sequence of a discretized Robosnail using direct waves to move upwards. The wave segment is the single faster-moving segment, while the remaining segments are the interwave. 61

4-5 Tractoring force - velocity relationship for robosnail 2. The graph shows various regimes of motion for robosnail 2, depending on tractoring force. At one extreme (far left), the applied load is so great that both the snail slips backwards, and there is slippage beneath the wave and interwave regions. At the other extreme (far right), the applied load is positive, and pushes the snail such that there is slippage forwards, against fluid drag forces beneath the snail. Between these two extremes there is a range at which the foot motions can propel the snail forwards without slippage at a velocity $\hat{V}_i$. Note that with zero Bingham number, we are left with the strictly Newtonian case, wherein no force can be generated by waving foot motions. 66

4-6 Tractoring efficiency for Robosnail 2, N = 6, varying the shear factor $1/S = \frac{\tau_i}{\tau_y}$. Curves shown for $B = 1, 2, 3, \ldots, 10$. The bottom curve is for $B = 1$. . 68

4-7 The first version of Robosnail 2 used shape-memory (Nitinol) wires to actuate the foot sections. This gave the advantage of compactness and minimized weight, but disadvantages were the slow and small movements of the segments (limited by the strain and cooling time required by the shape memory alloy) and the need for an umbilical cable. 70

4-8 Adhesive robosnail using multiple cylindrical cams. 71

4-9 Adhesive robosnail using a single cylinder cam. 72

4-10 Robosnail 2nd generation. 73

4-11 An exploded view of the internal transmission device of the second-generation Robosnail 2. The circular structure is the cam, surrounded by 6 followers. The followers each control one of the six foot segments in a linear motion. 74

4-12 Top and bottom views of the cam device. 74

4-13 Displacement per cycle of Robosnail 2a, on Laponite solution, 7.5 % by weight. The snail functioned the best on the horizontal, where gravity was not pulling against the direction of motion or away from the substrate. The worst performance occurred at 90 degrees vertical incline, when the snail had the greatest force resisting its motion. 76

4-14 Robosnail 2 tractoring force vs. normalized tractoring velocity. The working fluid is a Carbopol solution, 7% by weight. The measurements show good agreement with the tractoring force-velocity relationship derived earlier (equation 4.6) for a Bingham fluid with $\tau_y = 300$ Pa, $\mu = 300$ Pa s. The mass of the snail was 300 g, while the interwave velocity was 5 mm/s. The resultant Bingham number for these parameters is $B = 0.6$. 76

5-1 Motion sequence of three-link swimmer. 80

5-2 Hypothetical motion of the three link swimmer. The swimmer starts at "A", and flaps its right-side fin downward, moving the swimmer some x and y displacement Δx, Δy. From reversibility, this is the same as the reverse motion from B to C, and the sequence from C back to A is the same as the time-reverse mirror image from A to C. Thus we only need to know the motion from A to B to understand the full cycle. 81

5-3 Exploded view of three-link swimmer 83

5-4 The three-link swimmer. 83

5-5 Distance traveled for the three-link swimmer, normalized to total unfolded body length, as a function of the fin/arm lengths. (The curve shown is a best-fit polynomial is to guide the eye and not directly related to the theory.) 84

5-6 The three-link swimming next to fluid tracers. As the swimmer moves, it drags a portion of the fluid along with itself in the direction of motion, according to the no-slip condition, while simultaneously sending fluid backward in order to propel itself forward. As a result of fluid being forced forward and backward, the fluid is pulled in from either side of the swimmer, contracting lengthwise gridlines. 86

6-1 "Squishbot", a proposed flexible robot capable of changing size and shape. Such a robot will use flexible actuators and apply a method of locomotion similar to robosnail 2. Squishbot a joint project between MIT and Boston Dynamics, and is funded by the Defense Sciences Office at DARPA as part of the Chembots program. Artwork is from Boston Dynamics [2] 89

Chapter 1

Introduction

The realm of low-Reynolds number (Re) encompasses the world of the very small, the very viscous, or the very slow. If we were to shrink the size of a microbe, or to swim in a pool of honey, or to slow our motions to a snail's pace, we would catch a glimpse of this world. It would appear to us very alien because of the different physical laws that dominate. At this scale, the simple task of getting around involves strategies that are often counterintuitive and not applicable to the larger scales in which we live. Fortunately for us, it is not difficult to study this world, since varying the Reynolds number only requires changing characteristic speeds, lengths, or fluid viscosities, and not necessarily all three variables together. This way, we can understand microscopic systems by building a macroscale experiment and controlling the speed and/or fluid viscosity to achieve the correct Reynolds number.

Self-propulsion at low Reynolds number has been well-studied both theoretically and experimentally [44, 23, 4]. Observations of low-Reynolds number organisms suggest that the realm of low-Re requires a very different type of locomotion strategy. Most such swimmers do not resemble the macroscale (high-Re) swimming and flying organisms we are used to seeing. Instead of wings, fins, and flaps, we find mostly cilia and flagella as the dominant generators of propulsion [30, 19, 29]. One of the early researchers of low-Re locomotion was G. I. Taylor [47], who discussed the implications associated with flow reversibility at low-Re. Taylor also looked into the mechanics of flagellar propulsion, and built simple flagellar swimmers to demonstrate their efficacy. Another low-Re device, proposed by E.M. Purcell [41], was the hypothetical three-link swimmer, theoretically the simplest mechanism composed of rigid oscillating links capable of locomotion in the Stokes limit ($Re = 0$). While

Purcell proposed that such a swimmer should be able to generate a net displacement, no real prototype of this mechanism had been realized prior to this thesis.

While the locomotion of small mobile objects in an unbounded fluid at low-Re has been well-studied, the motion of organisms over a thin layer of fluid has been relatively less explored. This locomotion strategy has been adopted by a number of organisms including slugs and snails. Vlès [50] made one of the first detailed observations of the contractile motions of a snail's foot during locomotion. Decades later, Lissmann [31, 32] made detailed kinematic observations of the foot motions of snails and hypothesized certain ways that a snail might use a single foot to move over different surfaces. Denny [17, 18, 15], was the first to recognize that the non-Newtonian properties of snail mucus play an important role in locomotion. His careful studies of banana slug (*Ariolimax columbianus*) locomotion yielded valuable information concerning the interaction between the kinematics of the snail foot the and fluid dynamics of the mucus layer.

The research of snail locomotion has inspired a branch of low-Reynolds number locomotion based on peristaltic waves. It has been known that motions of boundaries over thin layers of viscous fluid can generate very large shear and normal stresses in the low-Re lubrication regime [42, 6]. While engineers have long taken advantage of these lubrication forces in the design of bearings, we sought to prove that, similarly, lubrication forces could be used for propulsion. To the best of our knowledge, until Robosnail 1, there has been no prior experimentation with free self-propelled peristaltic crawlers over thin fluid films.

1.1 Motivations

There are numerous emerging technologies that make use of low-Re flows and low-Re locomotion. Microfluidic devices, commonly known as "lab-on-a-chip" devices, are being developed to perform numerous fluid experiments (such as blood tests) using only a fraction of a sample droplet. Our understanding of low-Re flow will help us manipulate flows in such devices. As manufacturing methods become increasingly capable of creating and assembling micro-scale components, miniature swimming machines may be developed to navigate tiny fluid-filled passageways of the human body. A sound general theory of low-Re locomotion will be necessary to design and optimize these miniature swimming devices. The majority of this research has its focus on snail-inspired locomotion. Snails possess a mode of locomotion that is radically different from that of most other organisms. The simplicity of the gastropod foot (a single, continuous pad of muscle [36, 43]) suggests that one should be able to design similar simple machines capable of a variety of useful motions. As artificial muscle-like actuators become more widespread, they could conceivably be joined together easily to make simple snail-like actuators. Snail-like locomotion devices could be effective across a wide variety of substrates in the presence of viscous fluids. If the fluids are non-Newtonian, there can be further advantages, such as the ability to climb walls, which was one of the design goals of Robosnail 2.

In addition to micro-robotics, the field of oil drilling could potentially benefit from the application of snail-like devices. The setting of an oil well can be challenging as they are often muddy, vertical and irregular. A flexible slug-like or snail-like device may be more adept at navigating the fluid-filled environment of a downhole (the drilled hole in the ground of a potential oil site) than a more conventional rigid, jointed mechanism.

1.2 Snail locomotion

Many examples of soft propulsion systems can be found in the wild, particularly among worms and mollusks [49, 48]. With the exception of a few snails using cilia as a means of propulsion [13], snails moving on solid surfaces often display a similar pattern of undulations along the foot [35, 27, 25, 28] that may be in-plane compressions of the foot, or out-of-plane waving motions, depending on the species. It has been observed that certain species of flatworm [39, 40], earthworm [24, 14], polychaete worm [20, 34], and holothuroid (Echinodermata) [45] also generate peristaltic waving motions similar to that of snails during locomotion on flat surfaces.

What these animals lack in speed, they make up for in versatility. Terrestrial snails in particular are capable of climbing walls and ceilings, as well as traversing rough, irregular terrains, and are not hindered by wet surfaces. They accomplish this by carrying their own fluid lubrication, mucus. As the snail moves its muscular foot, the forces are transmitted to the substrate through the thin mucus layer. Thus the study of snail locomotion is a study of fluid dynamics, in which the viscous, non-Newtonian mucus and complex motions of the foot are optimized for the snail's unique mode of locomotion.

The most important property of mucus that allows a snail to exhibit such versatility in

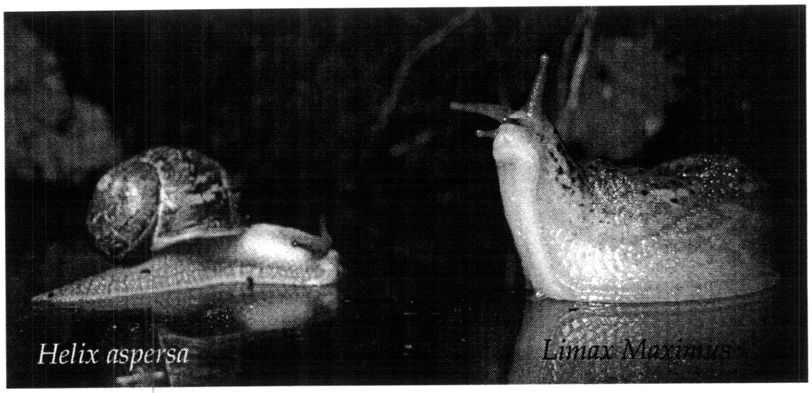

Figure 1-1: *Helix aspersa* and *Limax maximus*, two land snails which inspired the construction of Robosnail 2, the wall-climbing adhesive locomotion device. (Slugs are officially classified as snails)

locomotion is its finite yield stress. In other words, the mucus, even though it is more than 90% water, behaves as a solid unless it is stressed past a critical yield stress. The ability of the mucus to solidify allows a snail to maintain traction on a variety of surfaces, to climb walls, and to remain adhered to a wall or ceiling even when it is not moving.

While snail-like actuation systems have been built [26, 33]; to our knowledge, Robosnail 1 and Robosnail 2 [10, 11] are the first self-contained machines capable of propelling themselves in a manner analogous to live snails. We have constructed two types of mechanical snails: Robosnail 1 which uses a waving foot to move over viscous Newtonian fluids, and Robosnail 2 which uses a sliding foot to move over a shear-thinning fluid. The physical models of each locomotion method are distinctly different from one another. In terms of biomimicry, Robosnail 2 is the closest to the functioning of live snails, using adhesion and sliding rather than peristalsis and lubrication pressures as in the case of Robosnail 1. While Robosnail 2 is constrained by the limitation that it requires non-newtonian fluid to operate, it is capable of such feats as moving up walls or in an inverted position (see Figure 1-2). Both types of snail were explored in some depth, and the results are presented in chapters 3 and 4. It is likely that each mechanism will be adapted to its own type of application depending on the design constraints relating to the fluid dynamics of the application.

1.3 Three-link swimmer

The three link swimmer, like the robosnails, is the first machine of its type to be constructed. It is one of the simplest machines that theory predicts is able to swim in the Stokes limit.

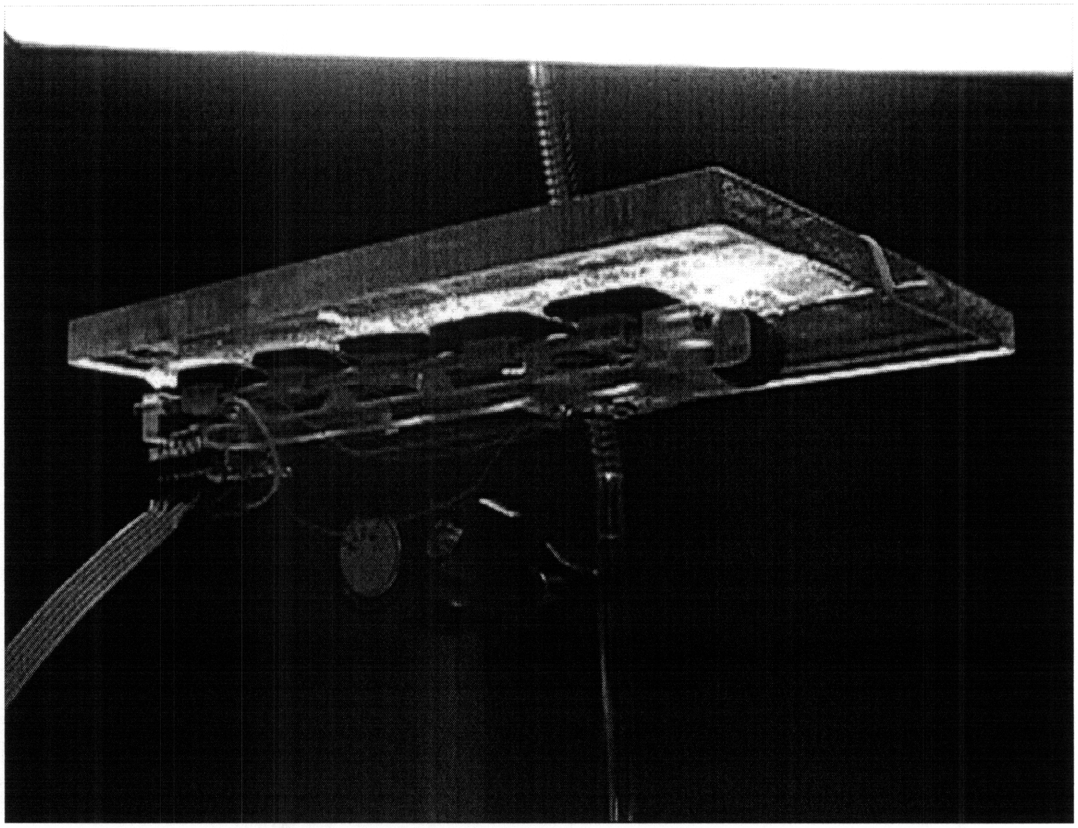

Figure 1-2: One prototype of robosnail 2, moving in an inverted position on a 1 mm layer of Laponite (A synthetic clay suspension)

Physically, it can be thought of as a free-swimming cousin to the peristaltic waving robosnail, where the waving motion is discretized into three rigid sections rather than a continuous, smooth wave. However, the three-link swimmer has given rise to further research into n-link swimmers which approach the continuous limit [46]. Because of the complex nature of the flow around the three-link swimmer, few equations are presented; however, the experimental results increase our understanding of the swimmer's behavior at low Reynolds number.

These devices together represent a diverse range of approaches to locomotion in viscous fluids, and have sparked a new generation of propulsive devices for locomotion at low Reynolds numbers related to the oil drilling and defense industries.

Chapter 2

General Theory

2.1 Locomotion at Low Reynolds Number

All of the systems described here operate at extremely low Reynolds number, the regime where viscous forces dominate over all inertial and buoyant forces. In this limit, the Navier-Stokes equations reduce to the Stokes equations. The Navier-Stokes equations for incompressible Newtonian fluids are given by

$$\nabla \cdot \vec{v} = 0$$

$$\rho(\frac{\partial \vec{v}}{\partial t} + \vec{v} \cdot \nabla \vec{v}) = -\nabla p + \mu \nabla^2 \vec{v} + \vec{f} \tag{2.1}$$

where ρ is the fluid density, $\vec{v}$ is the velocity field, p is the pressure, μ is the fluid viscosity, and $\vec{f}$ is an applied body force on the fluid.

The Reynolds number describes the relative magnitudes of inertial and viscous forces:

$$Re = \frac{\rho V L}{\mu} \tag{2.2}$$

where V and L are characteristic velocities and lengths in the flow. In the absence of body forces $\vec{f} = 0$, in the limit of low Reynolds number (approaching the Stokes limit where $Re = 0$, usually when V or L are small), the right-hand terms Navier-Stokes equation become zero, resulting in Stokes equations:

$$\nabla \cdot \vec{v} = 0$$

$$-\nabla p + \mu \nabla^2 \vec{v} = 0 \tag{2.3}$$

2.2 Lubrication Flows

When the fluid in question is constrained to flow inside a thin fluid gap, further simplifications can be made to the analysis. In this limit, the Stokes equations reduce even further to the lubrication equation:

$$\frac{\partial p}{\partial y} = 0 \tag{2.4}$$

$$\frac{\partial p}{\partial x} = \frac{\mu \partial^2 v}{\partial y^2} \tag{2.5}$$

where v the velocity of the fluid which flows only in the x- direction. Here the thin dimension of the film is aligned with y. The pressure of the fluid varies only along the direction of the film, and momentum effects are negligible.

2.3 Snail Locomotion

Consider a generalized snail consisting of a continuous, flexible foot, a means of actuating deformations of the foot, and a thin mucus layer of variable height, whose surface moves with a predefined cyclic motion. A point on the foot moves according to

$$\bar{u}(x,t) = \bar{u}(x - \hat{V}_w t), \tag{2.6}$$

where $\hat{V}_w$ is some waving velocity, and the wave shape is some periodic motion such that $u(x,t) = u(x+\lambda)$ where λ is the wavelength. Thus, while the foot is flexible and each point on the foot moves independently, the average velocity of any one point on the foot relative to the snail itself is zero:

$$\int_0^T \bar{u} dt = 0,$$

where T is the period of one cycle. While a mechanical or natural snail generally can have foot motions consisting of an arbitrary periodic deformation function $u(x, t)$, the two robosnails described here are special cases of the above. Robosnail 1 generates mainly height varying traveling waves whereas robosnail 2 generates mostly in-plane compression waves. Because these two modes of locomotion rely on distinct physical effects, they will be analyzed in separate sections.

The net force on the snail from the fluid is the integral of all the fluid forces acting on the foot. At the low Reynolds numbers involved, all flows can be considered quasi-steady, so acceleration terms are neglected:

$$F_t = \int_A dF = \int_A \tau dA + \int_A p dA$$

where F_t is the tractoring force (the force required to pull a given payload, or any given external force), A is the total area of the foot, τ is the shear stress in the fluid tangential to the foot surface, and p is the pressure within the fluid. Theoretically, a snail can generate propulsive forces from any combination of pressure and shear forces. In our case, we separate and test the two phenomenon separately: Robosnail 1 is a pressure-driven mechanism, while Robosnail 2 relies on shear forces for propulsion.

2.3.1 Shear-thinning fluids

While Newtonian fluids have a constant viscosity and therefore a linear response to increasing strain rate, non-Newtonian fluids typically have variable viscosity and a non-linear response. There exist numerous types of non-Newtonian fluids which can broadly be separated into shear-thickening fluids and shear-thinning fluids. Among the shear-thinning fluids there are numerous models, such as Bingham fluids (finite yield stress fluids), power-law fluids, and Herschel-Bulkley fluids (figure 2-1). Snail mucus is a shear-thinning fluid with some viscoelasticity, which can be modeled in several ways. The most important material property of the mucus that allows snails to move is the shear-thinning behavior. A shear-thinning fluid is one which has a viscosity that decreases with increasing shear rate. Figure 2-2 shows the shear stress - viscosity relationship for Carbopol, the main fluid used to test Robosnail 2. Carbopol is a synthetic thixotropic fluid, chosen for its rheological similarity to real snail mucus.

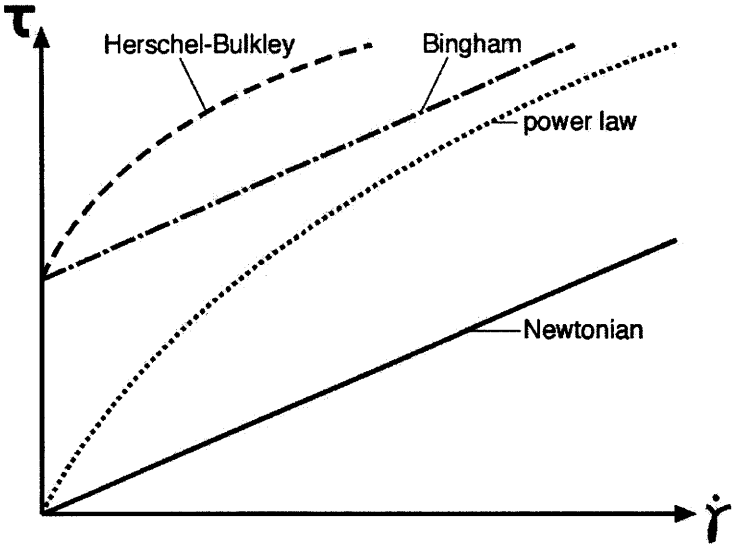

Figure 2-1: Shear-rate ($\dot{\gamma}$) versus shear-stress (τ) curves for various fluids. Robosnail 2 exploits the physical properties of non-Newtonian fluids and theoretically can use any of the fluids shown, except for the Newtonian fluid. The four fluids shown above have simple mathematical representations: For the Newtonian fluid $\tau = \mu\dot{\gamma}$, for the power law fluid $\tau = \mu\dot{\gamma}^n$, for the Bingham fluid $\tau = \tau_y + \mu\dot{\gamma}$, and for the Herschel-Bulkley fluid $\tau = \tau_y + \mu\dot{\gamma}^n$.

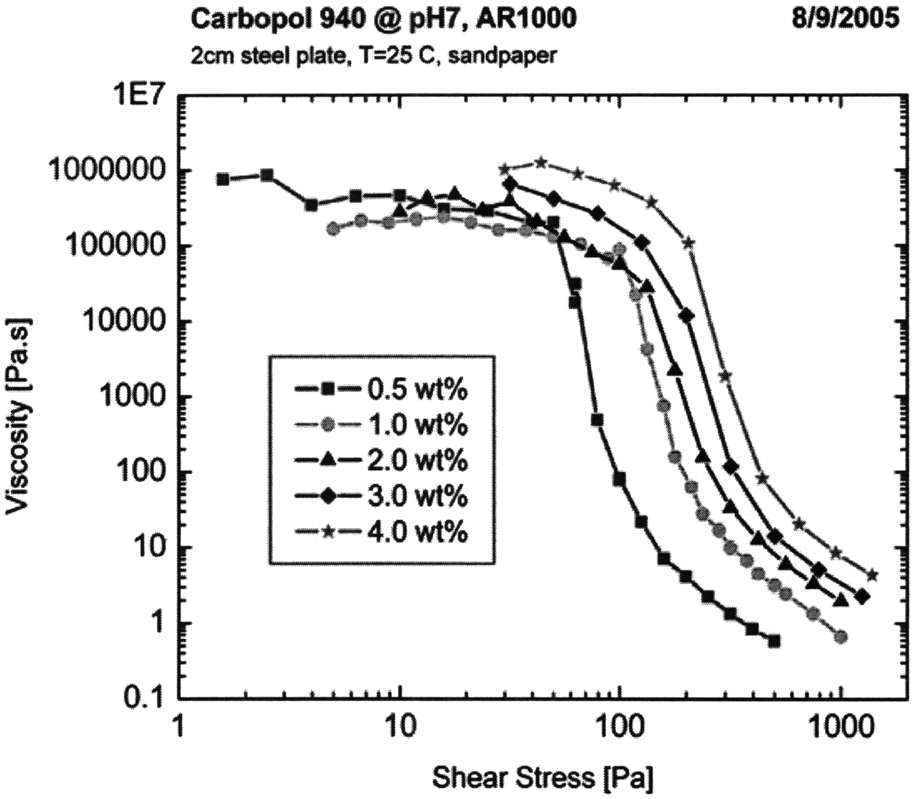

Figure 2-2: Shear-rate versus viscosity curves for various concentrations of Carbopol, a synthetic fluid used for the lubrication layer of Robosnail 2 [21, 22]. Note that for each curve, the viscosity drops several orders of magnitude beyond a certain shear stress. This is the shear-thinning behavior; Newtonian fluids possess a constant viscosity regardless of shear rate. This shear-thinning behavior is a critical property that allows Robosnail and most live snails to move. When approximated as a finite yield-stress fluid, the yield stress can be taken as the point at which the viscosity drops off. (Figure appears courtesy of Randy Ewoldt [21])

Two secondary properties that affect snail locomotion are the finite yield stress and the restructuring time. Carbopol and snail mucus, for our purposes, can both be classified as finite yield stress fluids. It is this finite yield stress, as opposed to general shear-thinning behavior, that allows the snail to move upside-down on smooth surfaces, and to passively glue themselves to vertical or inverted surfaces when they are stationary. This is possible because the fluid has a range of stresses under which the fluid effectively remains solid, gluing certain parts of the snail's foot onto the substrate.

More accurately, natural snail mucus does not have a truly solid state, but instead, a high viscosity (in the "unyielded" regime) where the viscosity is many orders of magnitude higher than in the "yielded" regime. The high viscosity is so great and the resultant flow rates so low that the fluid can practically be considered "solid-like". Synthetic analogs of snail mucus, such as Laponite and Carbopol, likewise have a pronounced shear-thinning behavior that can be treated as a having a finite yield stress.

Chapter 3

Robosnail 1

3.1 Introduction

Many organisms use undulation as a means to move through fluids, or to transport fluids. Robosnail 1 was built with the intention of emulating peristaltic crawlers, using a flexible, powered foot to move over a thin layer of viscous Newtonian fluid. As we shall see in the following chapter, this type of crawling is more "snail-inspired" than "snail-like." In reality most snails use a different mode of locomotion (that we explore with the Robosnail 2 prototypes in Chapter 4). Regardless of its relevance to live snails, peristaltic lubrication propulsion has proven to be an effective mode of transportation.

The basic idea behind robosnail 1 is to use a waving sheet to squeeze viscous fluids backwards through the thin gap between snail and substrate. The reaction force of the fluid on the snail propels the snail forwards. Our initial prototype machines undulated a thin rubber foot over a layer of glycerol, propelling themselves at a velocity close to the speed of the undulating traveling wave.

3.2 Theory

3.2.1 Underlying physics

Robosnail 1 locomotion is analogous to the peristaltic pumping observed in the movement of fluid through the intestine is due to the peristaltic motion of the intestinal wall. In Robosnail 1, the foot is analogous to the pumping wall, and as with peristaltic pumping, the wall exerts a force on the fluid. The fluid in turn transmits a force on the substrate which, unlike peristaltic pumping causes motion of the pumping device. The changing shape of the snail foot is described by the fluid thickness height $\hat{h}(x,t)$, which varies with time (see Figure 3-1). For simplification of the analysis, we assume that the waving membrane is periodic with a wavelength λ such that $\hat{h}(x,t)$ =$\hat{h}(\hat{x}+n\lambda,t)$ and that the waves travel with a speed $\hat{V}_w$ such that $\hat{h} = f(\hat{x} - \hat{V}_w t)$. We define the average height $\hat{H} = \frac{1}{\lambda}\int_0^\lambda(\hat{h})dx$ and an amplitude $\hat{a} = \hat{H} - min(\hat{h})$. The snail travels at some resultant velocity $\hat{V}_s$. For practical concerns, the crawler may also be transporting some payload (or tractoring force) with resultant load $\hat{F}_t$.

Natural mucus used by snails is a viscous, non-Newtonian fluid which has a variable viscosity dependent on shear rate. As shown in later chapters, real snails exploit these non-Newtonian properties in their method of locomotion and their motion would be severely handicapped if their mucus were Newtonian. However, because robosnail 1 relies on Newtonian effects, the 'mucus' used with Robosnail 1 can be a viscous Newtonian fluid, and will be modeled as such. Since the layer of fluid is thin, we assume that the lubrication approximation holds everywhere in the fluid film. Under this assumption, pressure varies in the $x-$ and $y-$ directions, but not in the $z-$ axis. In this limit, the Navier-stokes equations reduce to the lubrication equation, which is the $x-$component of the Stokes equation:

$$\mu\frac{\partial^2 u}{\partial z^2} = \frac{\partial \hat{p}}{\partial \hat{x}}.$$

At this point it becomes useful to non-dimensionalize the equations, rescaling the relevant quantities as follows:

$$\hat{x} = \lambda x$$

$$\hat{z} = \hat{H} z$$

$$\hat{u} = \hat{V}_w u$$

$$\hat{p} = \frac{\lambda\mu\hat{V}_w}{\hat{H}^2} p$$

$$\hat{h} = \hat{H} h$$

$$\hat{V}_s = \hat{V}_w V_s$$

and

$$\hat{F}_t = \frac{\lambda^2 \mu \hat{V}_w}{\hat{H}^2} F_t$$

The lubrication equation then becomes:

$$\frac{\partial^2 u}{\partial z^2} = \frac{\partial p}{\partial x}$$

in dimensionless form.

For thin profiles, pressure does not vary across the depth of the film. Hence, for any given x-position, the pressure is constant. The flow profile then must be parabolic for any value of x, taking the form

$$u(z) = \frac{\partial p}{\partial x} z^2 + C_1 z + C_2 \tag{3.1}$$

where the integration constants C_1 and C_2 are determined by boundary conditions at the foot and the substrate. To solve for these constants we switch to a reference frame traveling with the wave. In this frame, the height function of the foot $h(x)$ does not vary with time. Because the flow is steady, the volume flow rate $Q = \int udz$ (per unit width) is a constant. The top and bottom surface velocities in the new reference frame are:

$$\hat{V}|_{z=0} = \hat{V}_w - \hat{V}_s$$

$$\hat{V}|_{z=h} = \hat{V}_w$$

or in dimensionless terms,

$$u|_{z=0} = 1 - V_s$$

$$u|_{z=1} = 1.$$

Applying these boundary conditions to equation (3.1), the velocity profile becomes

$$u(z) = \frac{1}{2}\frac{\partial p}{\partial x} z(z-h) + V_s(\frac{z}{h} - 1) + 1 \tag{3.2}$$

Integrating $Q = \int_0^h udz$ and solving for $\frac{dp}{dx}$ we find

$$\frac{dp}{dx} = \frac{12}{h^3}[h(1 - \frac{v_s}{2}) - Q]. \tag{3.3}$$

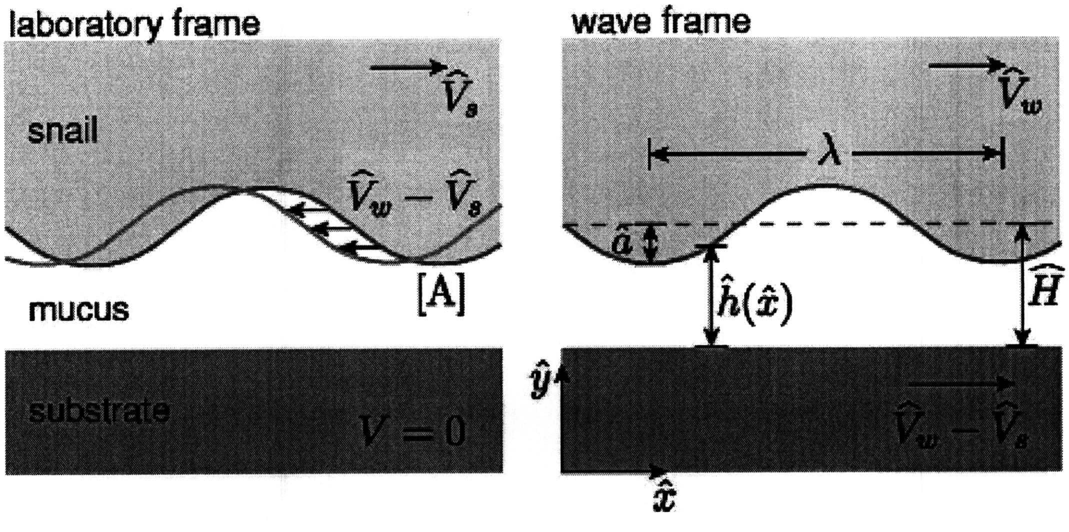
laboratory frame
$\widehat{V}_s$
snail
$\widehat{V}_w - \widehat{V}_s$
[A]
mucus
substrate
$V = 0$
wave frame
$\widehat{V}_w$
λ
$\hat{a}$
$\hat{h}(\hat{x})$
$\widehat{H}$
$\hat{y}$
$\widehat{V}_w - \widehat{V}_s$
$\hat{x}$

Figure 3-1: Switching to a moving reference frame to find the flow underneath a self-propelled, peristaltic waving membrane. In the laboratory frame, the foot height is a function of x and t. In the wave frame (a frame of reference following the wave crests) the height is only dependent on x and the flow can be modeled as steady.

Applying the periodic boundary condition

$$\int_0^1 \frac{dp}{dx} dx = p(1) - p(0) = 0$$

integrating (3.3) and solving for Q gives

$$Q = (1 - V_s/2)\frac{I_2}{I_3} \tag{3.4}$$

where

$$I_j \equiv \int_0^1 \frac{dx}{h^j}.$$

Forces come from the viscous shear at the surface of the membrane, and from the high pressure zones where the foot is nearly touching the ground. The shear forces act parallel to the foot surface, and the pressure force acts perpendicular to it. We are mainly concerned with forces in the x- direction (vertical forces depend on the average pressure under the foot, which can vary arbitrarily by a constant of integration).

The total dimensionless force acting on the foot is given by

$$F = F_{pressure,x} + F_{shear,x} = \int_0^1 \left(p\frac{dh}{dx} + \frac{du}{dz}|_{y=h} \right) dx.$$

Integrating the pressure term by parts and substituting (3.3) for $\frac{dp}{dx}$ yields

$$F_{pressure,x} = \int_0^1 p\frac{dh}{dx}dx = \left(12I_1 - \frac{I_2^2}{I_3}\right)\left(1 - \frac{V_s}{2}\right) \tag{3.5}$$

Substituting Q from equation (3.4) gives the relation between the velocity and the tractoring force of the snail:

$$V_s = \frac{6(1-A)}{4-3A} - \frac{F_t}{I_1(4-3A)} \tag{3.6}$$

where the shape function

$$A \equiv \frac{I_2^2}{I_1 I_3}.$$

The relation between force and velocity takes the simple linear form of $f = f_{stall} - mV_s$ where f_{stall} is the stall force, and m is a constant. Their respective values can be found by rearranging terms in equation (3.6):

$$F_{stall} = 6I_1(1-A) \tag{3.7}$$

$$m = -I_1(4-3A) \tag{3.8}$$

When $V_s = 0$ the force reaches the stall force. As the applied force on the snail is decreased, the velocity increases linearly until it reaches the free velocity, $V_{s,free}$

$$V_{s,free} = \frac{6(1-A)}{4-3A} \tag{3.9}$$

Figure 3-2 illustrates this straightforward relationship, which can be used to predict the snail's resultant velocity given any applied force. The free velocity and dimensionless stall force, F_{stall}, are both purely functions of the foot shape, through I_j and A. For a sinusoidal foot, the foot shape is determined by a single dimensionless parameter, a or the ratio of amplitude to average height above the substrate. This is a practical parameter that quantifies how close the foot is to the ground, and is limited by $0 < a < 1$, that is to say, the wave can be completely flattened setting $a = 0$, or touching the substrate when $a = 1$. In most engineering applications, one would like to maximize the stall force of a robosnail. The simplest way to increase the stall force is revealed by equation (3.8)- by decreasing the clearance between the foot and the ground. Other methods include increasing the number

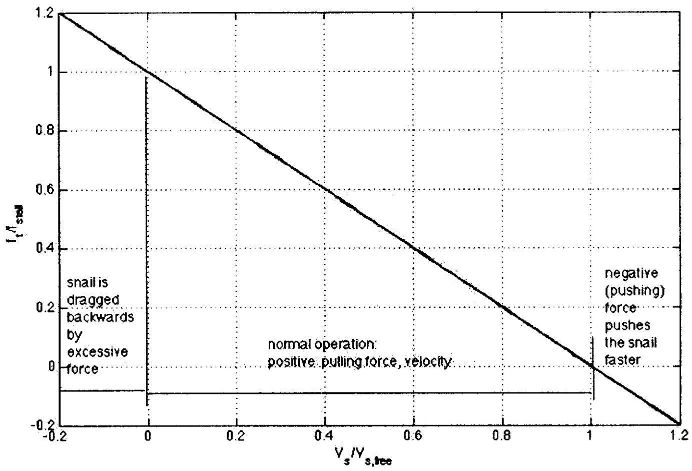

Figure 3-2: (Left) The relationship between dimensionless applied force and snail velocity. As the tractoring load is increased to the stall force, the velocity decreases to zero. The full graph extends past $f < 0$, where increasing the tractoring force beyond the stall force would cause the snail to drift backwards, and $V_s > V_{s,free}$ where a negative (pushing) tractoring force would increase the snail velocity past $V_{s,free}$.

of waves created by the foot, or increasing the viscosity of the working fluid, all of which are proportional to the dimensional stall force.

Note that the resultant dimensionless force and velocity are merely a function of the wave shape. This is analogous to the Stokes flow generated by self-propelled objects in an infinite fluid in which the objects' motion is only a result of the geometry. For the snail, the problem is even more simplified, as the velocity and force can be analytically predicted as long as the height $h(x)$ is an integrable function.

3.2.2 Various wave shapes

As equation (3.6) shows, the force and velocity relation is a function of the height profile, which has been left in the general form $h(x)$. Thus any number of height profiles can be used, theoretically, resulting in a different force-velocity curve for each one. The easiest way to change the dimensionless height profile is to vary the amplitude with respect to the offset height. Figure 3-3 shows the dimensionless free velocity as a function of dimensionless amplitude for a variety of waving profiles. Note that for some profile shapes, such as the triangle wave, we obtain a counterintuitive result where the expected snail velocity is greater than the undulating velocity.

To understand the increase in speed associated with sharp waveforms, consider the

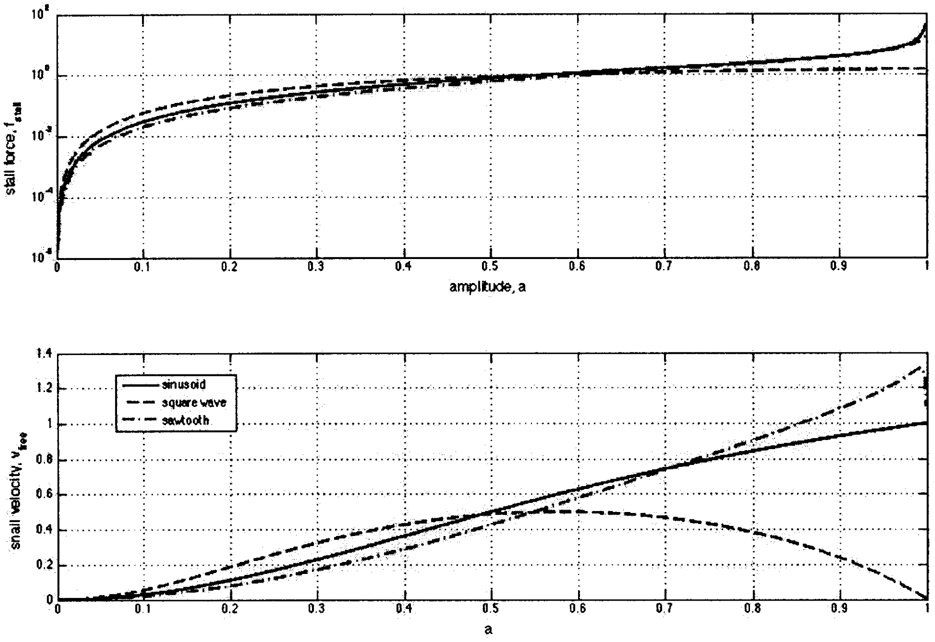

Figure 3-3: Dimensionless stall force and free velocity for a three different wave shapes: sinusoid, sawtooth, and square. Note that the force is displayed on a log scale. As the amplitude gets larger, with the foot nearly touching the substrate, lubrication pressures increase, and the stall force increases rapidly. While the stall force is similar for the three wave shapes across the given range of amplitudes, there is significant variation in the free velocity ([10]) for differing wave shapes. The square wave performs favorably at low amplitudes, but as the amplitude nears $a = 0.5$, the sharper wave profiles gain an advantage. Note that the model predicts that the sawtooth wave can achieve $\hat{V}_s > \hat{V}_w$

interaction of the foot and the thin fluid layer. Upon close inspection, we find that the extra "boost" in pressure force for the triangle wave arises near the lowest extremities of the waveform. When the wave shapes approach the substrate, the pressure buildup and hence the majority of propulsive force comes from the area immediately surrounding these minimum points. The velocity of a snail with a sinusoidal wave profile approaches the waving velocity as the waves near the substrate; but a snail with a sharp waving profile should move even faster. Near the touchdown points, the surface is more vertical to take advantage of the pressures propelling the snail, furthermore, there is less surface in close proximity to the ground, so the viscous drag is reduced.

To further explore this effect of sharp waveforms, we consider additional shapes besides the sinusoid and triangle wave. In particular, we are interested in waveforms which have lower extremity shapes that fall somewhere between the "smooth-bottomed" sinusoid and the "sharp-bottomed" triangle wave. Of course, there are an infinite number of wave shapes we can consider, as almost any arbitrary repeating shape can be made into a wave profile. However, it is primarily the shape of the lower points that determines the crawling velocity, so we wish to find a wave type accordingly whose sharpness we can vary with ease. One simple solution is to replace the sinusoid with two parabolas, one opening upward and one opening downward. The advantages of this approach are that there are no slope discontinuities to disrupt the force equation, and we can vary the sharpness by changing the sharpness factor f_s, the ratio of width of one parabola to the entire wavelength. As f_s approaches 1, the second parabola reduces to nothing, and the waveform becomes a repeating inverted parabola. While this is not exactly a triangle wave, it should behave much like one, since the low areas resemble the triangle wave's sharp point, and the majority of the propulsive force is generated in this area. We would like to determine at which f_s the snail starts to move faster than its own waving speed.

Since the velocity is a function of wave shape only, we use the velocity equation (3.9) and solve for free velocity as a function of the foot nearing the substrate (expressed as a variable amplitude a but defined for the irregular wave shape as $h_0 - h_{min}$ so that the geometry is normalized as with the sinusoidal case). The solution for the free velocity as the foot approaches the substrate, for various "sharpness ratio" f_s is shown in the figure 3-5. The "overdrive" phenomenon occurs roughly at a ratio of $f_s = 0.7$ and an amplitude of $a = 0.85$.

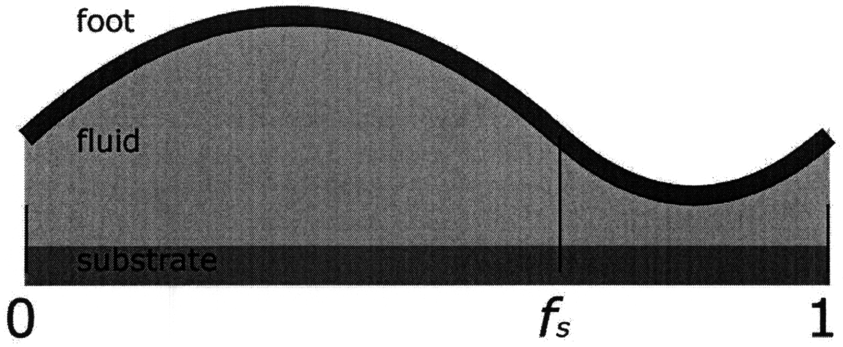

Figure 3-4: A “composite” waveform made of two parabolas. By varing the sharpness factor f_s (the relative size of the downturned parabola to the entire wavelength) from near 0 to near 1, we can vary the free velocity as a function of the amplitude.

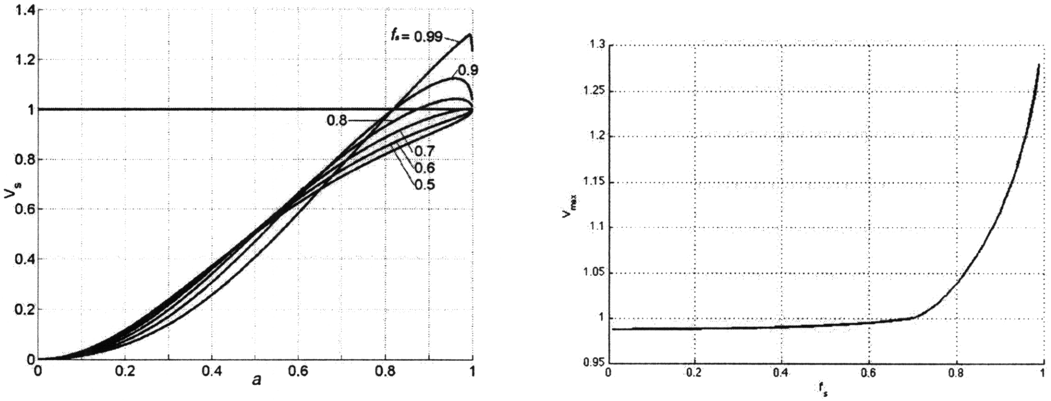

Figure 3-5: (Left) Dimensionless velocity as a function of the “sharpness ratio” of the two parabolas composing the wave. $\hat{V_w}$. (Right) Maximum velocity attainable as a function of the sharpness ratio f_s. As the lower parabola becomes less than 30 percent of the total wavelength ($f_s = 0.7$), the snail begins to move at a speed greater than the waving speed

3.2.3 Three-dimensional effects for a finite-width snail

The two-dimensional theory is sufficient to explain how peristaltic motion of a membrane over a thin viscous fluid can propel itself. However, in most real-life situations requiring robosnail-like motion, the snail has finite width, resulting in edge effects that cause a discrepancy between the two-dimensional theory and full three-dimensional results for force and velocity. At the edges of a finite-width waving sheet, the lubrication pressures underneath the waving sheet in regions near the edges are diminished as fluid is allowed to leak to and from the region outside of the thin gap. Since the propulsive force is an integral of the pressure forces on the foot, we expect there to be losses in the propulsive force. Conversely, we would not expect equivalent shear losses, because shear stresses do not "leak" as pressure does. Hence the overall expected result of imposing finite-width conditions would be decrements in the towing force, free velocity, and efficiency. This is verified by both numerical simulations and experiments.

Due to the complexity of the three-dimensional flow in the gap of varying height, we found no analytical formulation to describe the pressure field under a finite-width sheet. However, we were able to numerically solve for the flow and pressure field using the three-dimensional lubrication equations which, like two-dimensional lubrication, remain valid as long as the Reynolds number is sufficiently low and the gap height is sufficiently small compared to the wavelength:

$$\frac{\partial p}{\partial x} = \frac{\partial^2 u_x}{\partial z^2}$$

$$\frac{\partial p}{\partial y} = \frac{\partial^2 u_y}{\partial z^2}$$

These lead to a differential equation

$$-\nabla^2 p = 3\frac{dh}{dx}\frac{\partial p}{\partial x}\frac{1}{h} + 12\left(1 - \frac{V_s}{2}\right)\frac{dh}{dx}\frac{1}{h^3} \tag{3.10}$$

which is solved numerically.

In the simulation, the foot was divided into discrete segments over one wavelength with boundary conditions of periodicity between the front and rear edges, and pressure falling to zero at the side edge. The pressure was calculated, as well as the net propulsive force,

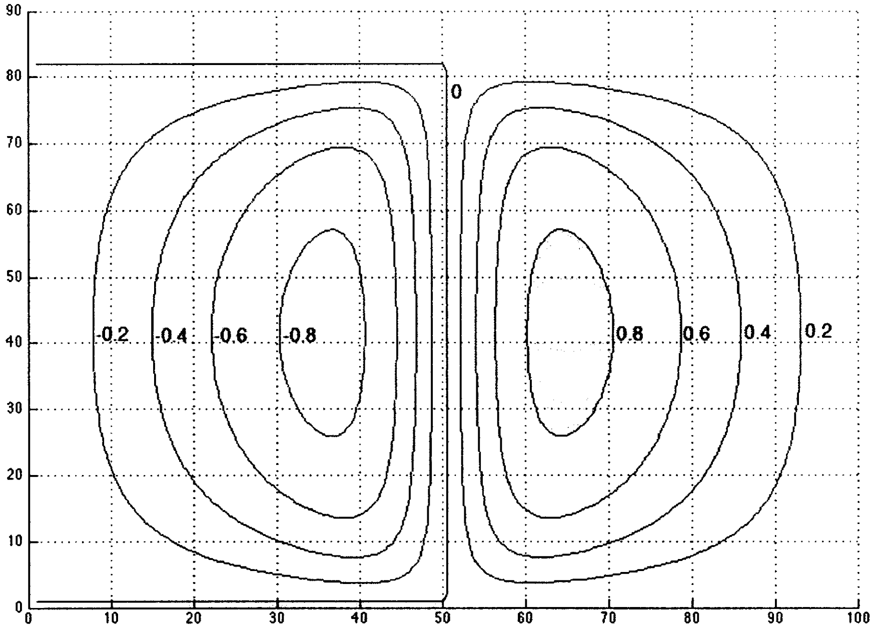

Figure 3-6: A typical Matlab simulation result of pressure underneath a finite width, periodic waving robosnail 1 foot, with an aspect ratio of $b = W/\lambda = 1.6$ and $a = 0.7$. The simulation itself uses a periodic end conditions in x and is mirrored along the x-z plane. The waving foot generates a pressure similar to the two-dimensional waving robosnail foot near the centerline, but at the edges, the fluid is allowed to leak, and pressure decreases, decreasing the total propulsive force.

which is the integral of the pressure forces in the direction of travel. The velocity was found in a manner analogous to the two-dimensional case. Figure 3-6 shows a representative plot of pressure over the surface of the foot.

The resultant force-velocity curves and pressure profiles were compared to the two-dimensional case with identical amplitude and height parameters. Simulations predict that the finite-width snails do not perform as well as the infinite case, matching our expectation. As we increase the snail width, the fluid has less opportunity to leak and the profile begins to resembles the 2D case. Figure 3-8 compares the ratio of stall force in 3D to the expected stall force in the 2D case while varying the foot width from near zero, two several times the wavelength. We see that for a given snail foot width, wave profiles that are closer to the ground have higher force - closer to the 2D prediction - compared to wave profiles that ride higher. Intuitively this makes sense as the fluid trapped in the small space between wave and ground is less susceptible to leakage than the fluid underneath a larger space. At

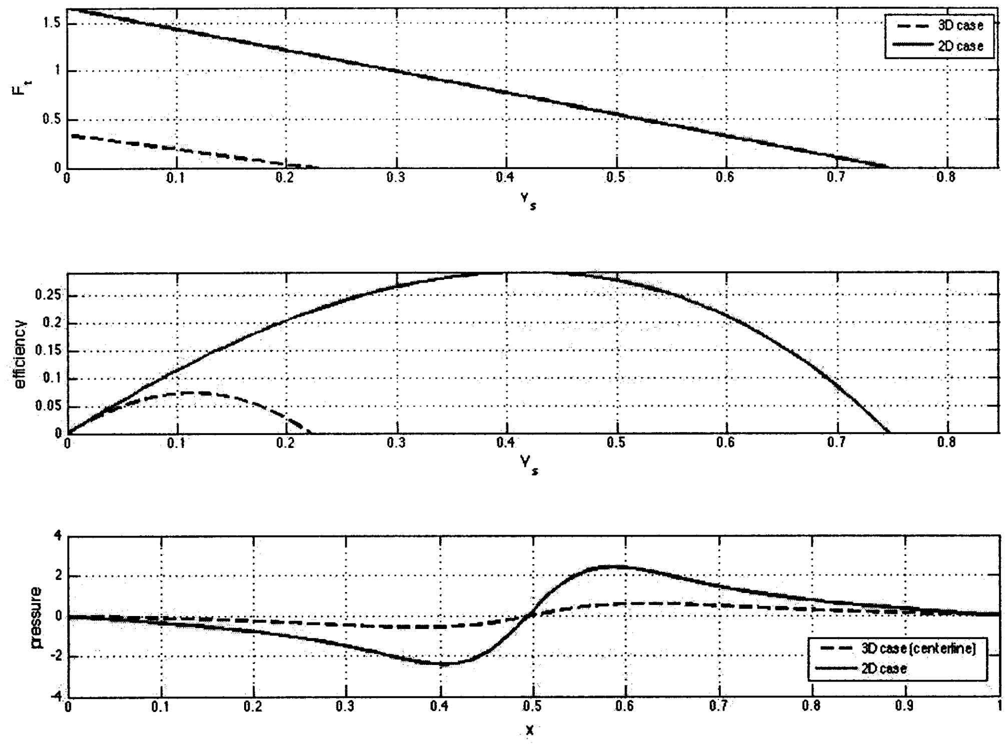

Figure 3-7: Tractoring force, snail velocity, and centerline pressure plot for robosnail 1, comparing a finite width snail with an infinitely wide snail. The finite snail has a waving amplitude a 0.7 times the average fluid film height, and a width W equal to 0.8 times the wavelength λ. The wave shapes for both cases are the same. The finite snail suffers from edge leakage, which degrades the maximum tractoring force and velocities, as well as the efficiency. The centerline pressure serves as a qualitative evaluation of how much propulsive pressure is lost overall in the finite case.

lower amplitudes of $0 < a < 0.1$, the snail's 3D to 2D force ratio asymptotes to a single curve. This lower limit of force at low waving amplitudes suggests that the propulsive force is generated over a large area of the foot rather than concentrated spots along the low areas, and as the edge leakage affects the wider gap areas of the foot, the entire pressure field is affected by the leakage at these small amplitudes.

For all of the finite width cases (and with the experiments to be described in the following section), the analysis was done with the foot edges open to the fluid without any type of sealing. We expect a partial seal could be created with a wall that extends near to the substrate to hold in some of the pressure. One might expect some optimal separation between sealing wall and substrate where the pressure could be contained appreciably while

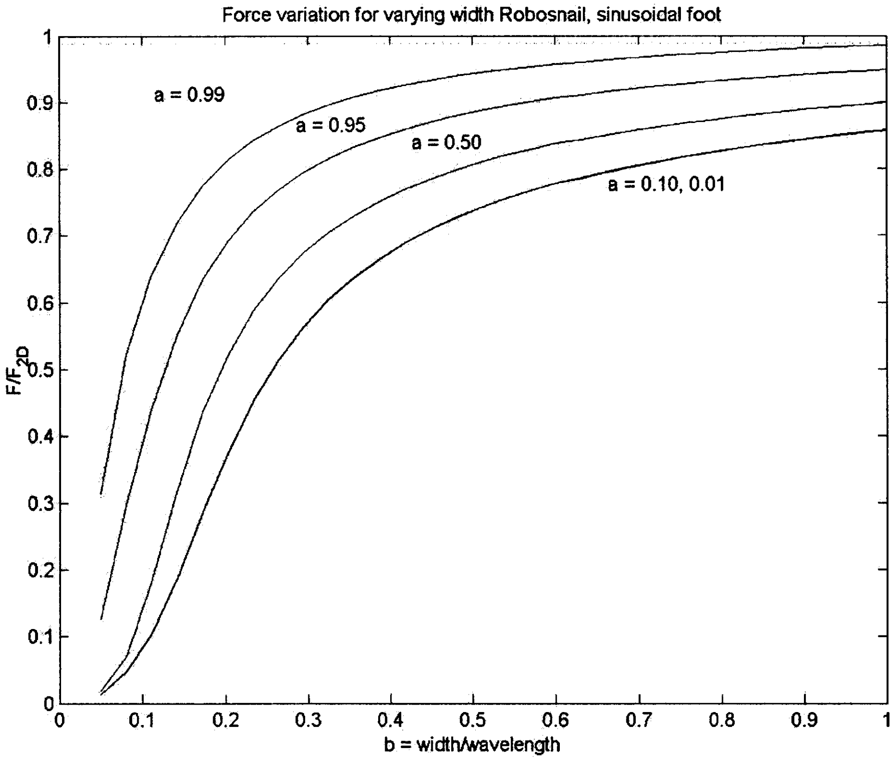

Figure 3-8: Simulation results showing ratio of tractoring force for a finite-width robosnail compared to the same robosnail 2D analytical result, with sinusoidal wave profile. Note that below $a < 0.1$ the expected force ratio asymptotes to the lowest curve.

the shear stress losses in the fluid gap between the edge of the sealing wall would not be so great as to nullify the benefits of the seal. Another way to improve performance, aside from building a wide snail, is to run the system inside a cylindrical environment, and to have the peristaltic motion of the foot generate waves in the axial direction inside the cylindrical hole (or around the outside of a cylindrical rod). This way, there are no edge effects except at the leading and trailing edges, and if the thickness of the fluid layer is small in comparison with the radius of the rod, the fluid flow and forces can be analyzed using the 2D method.

3.2.4 Power and efficiency

The input power to a Robosnail device can be readily calculated with a simple integral. For every section of foot, the differential amount of force exerted is equal to the pressure in the fluid times the differential area. For thin fluid layers, we can imagine the foot as being actuated by numerous small linear actuators, each feeling a resistance force of

$$dF = PdA = bPdx.$$

The differential power exerted is the differential force times the vertical waving velocity at that point.

$$d\dot{W}_{in} = V_y dF = V_y bpdx$$

$$\dot{W}_{in} = b\int_0^L V_y pdx.$$

Recall, however, that $V_y = V_w \frac{dh}{dx}$, so that

$$\dot{W}_{in} = V_w b\int_0^L \frac{dh}{dx} pdx.$$

Since $\hat{F}_{x,p} = b\int_0^L \frac{dh}{dx} pdx$, the power expended simplifies to the expression

$$\dot{W}_{in} = V_w F_{x,p}. \tag{3.11}$$

The efficiency of the snail is the ratio of useful power to the power expended:

$$\eta = \frac{\hat{V}_s F_t}{\hat{V}_w F_{x,p}} = \frac{V_s F_t}{F_{x,p}}. \tag{3.12}$$

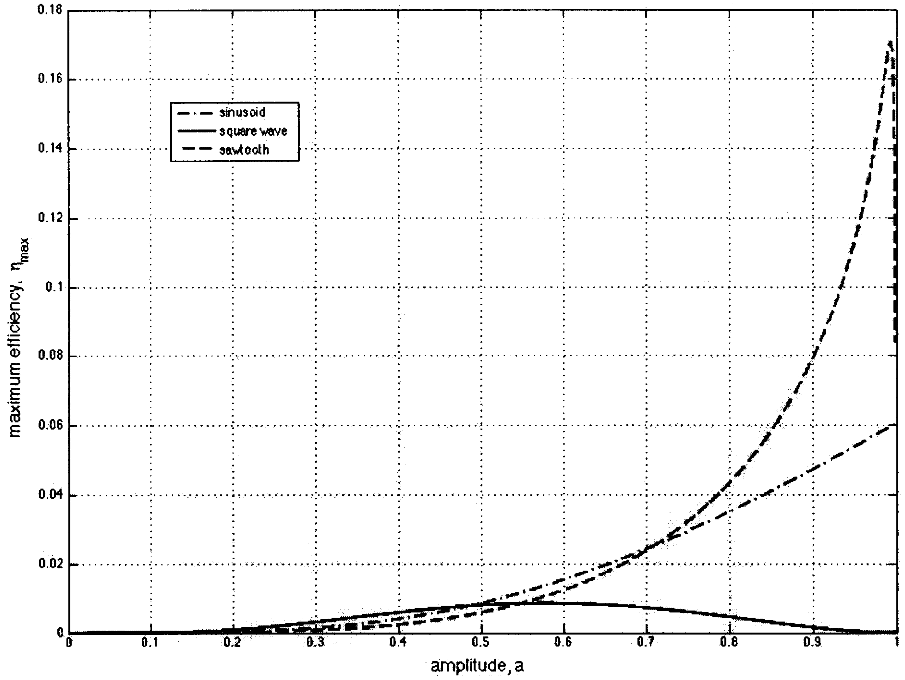

Figure 3-9: Maximum efficiency plot of a 2D robosnail with various wave shapes and over a range of amplitudes. The relative efficiency performance of the three wave shapes is comparable to that of the free velocity (Figure 3-3).

In the 2D case, we can substitute the expressions for the horizontal pressure force (3.5) and snail velocity (3.6) to find an analytical expression for the efficiency as a function of snail velocity:

$$\eta_{2D} = \frac{I_1 V_s[6(1-A) - V_s(4-3A)]}{\left[12I_1 - \frac{I_2^2}{I_3}\right]\left[1 - \frac{V_s}{2}\right]}. \tag{3.13}$$

In general, we find that the efficiency curves of various wave shapes to behave in a similar fashion to the free velocity curves of the same wave shape - if a certain wave shape has a higher free velocity at a given amplitude than another wave shape, we can expect that it would also have a higher maximum efficiency (figure 3-9). It becomes clear that at different waving amplitudes, different wave shapes are optimal. The question of optimality has been studied analytically for the waving sheet [52, 51]

In three dimensions, the snail velocity and pressures can be found numerically. Figure 3-7 compares the efficiency for a the 2D case and a typical 3D case, where the snail width is 0.8 times the wavelength. The wave shapes for both cases are the same. The finite-width snail generally experiences a lower efficiency than its 2D counterpart, as we had expected.

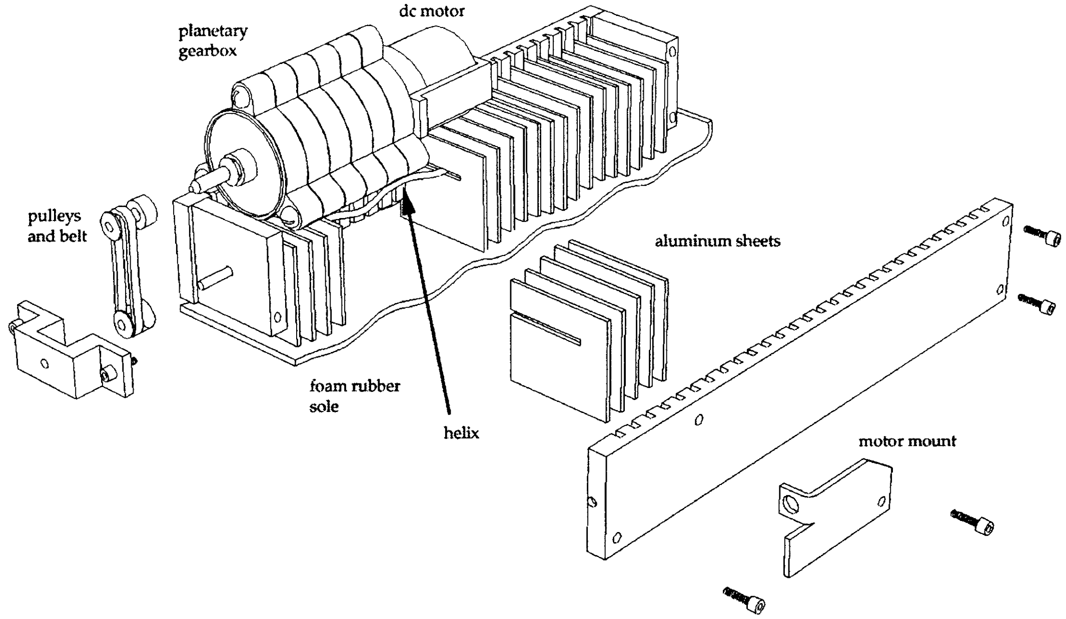

Figure 3-10: Partially exploded view of Robosnail 1 showing motor/gearbox assembly, rotating helix, slot plates, and membrane.

3.3 Mechanisms

One of the simplest wave shapes that can be generated with the waving foot is a sinusoidal wave. To do this, we used a shallow helix threaded through slotted plates which are constrained to move vertically (see figure 3-10). The bottom edges of the rectangular plates are affixed to a flexible membrane. Each of the plates then acts as a connecting rod, with its section of helix acting as a crank, transferring the vertical component of its rotational motion to its section of the membrane. The helix was driven by a geared-down motor. The resultant motion of the rotating helical crank is a traveling sinusoid along the length of the membrane with a wave speed (cm/s) equal to the wavelength (cm) divided by the rotations per second (1/s).

A handful of designs were proposed for the construction of a peristaltic robosnail that could mimic any waveform, but of the few that were built ultimately none of the designs tested were reliable enough to generate useful data. One of the main challenges was to create a device with high enough resolution to emulate the sharp waveforms that are of the most interest. Many of the devices required a large number of linkages each connected to a cam follower, but the complexity of the systems made construction of such devices prohibitively difficult. However, the designs are briefly described here for the sake of discussion and completeness.

One cam-driven robosnail that was built (see figure 3-11) involved an interchangeable cam which could accommodate up to 64 cam followers. The membrane was wrapped around in a circle concentric with the cam, so the motion of the snail (or the fluid, as the tank was built to rotate) was in a circle concentric with the apparatus. This was done for two reasons: 1) to simplify the machine, 2) to make the waveform periodic, and 3) to reduce leakage from the sides of the membrane. As long as the width of the snail is sufficiently small compared to the mean diameter of the membrane, the 2D theory is still applicable. The experiment yielded little useful data, as the membrane was barely wide enough to generate force, and there were significant losses due to friction in the bearing supporting the tank, so the tank rotated much less than the 2D prediction.

The analysis was further complicated by the fact that the tank walls inhibited some of the pressure loss, so while the snail was far from the ideal infinite case, the results could be directly compared to neither the ideal 2D case nor the 3D simulations, which described a free fluid with no side walls. The snail also suffered from high friction at the cam followers, even with only 8 followers installed; this suggests that the mechanical losses with a larger number of followers would play a dominant role in determining "crawling" velocities.

Another proposed method to generate arbitrary waveforms was to use a semisolid belt with waveform "chunks" attached on the outer surface. The belt would run against a stretched membrane so that its shape would be transferred onto the membrane while the surface of the membrane would remain more or less at a constant place rather than being pulled along with the belt. A similar idea involved using screwlike rollers to transfer a sharp trough wave profile onto a membrane with lateral stiffness members (see figure 3-13). As all of these proposed devices involved rubbing a tensioned membrane against a moving form, it is doubtful that we could build an effective device with enough tension in the membrane to hold it against the form to counteract the high pressures at the wave troughs, while maintaining a low enough friction force between the moving form to run reliably. We concluded that a system using cams and actuators would likely be more efficient albeit harder to construct.

In the end, the helix-driven sinusoidal robosnail 1 models were the most reliable versions and will be the focus of this study.

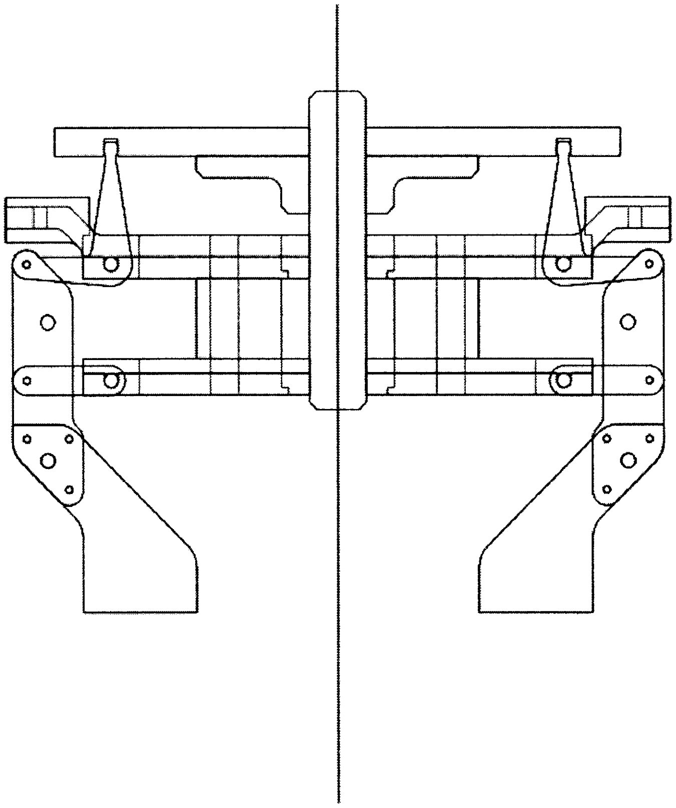

Figure 3-11: Side cross-section of the “ring snail” with interchangeable cams

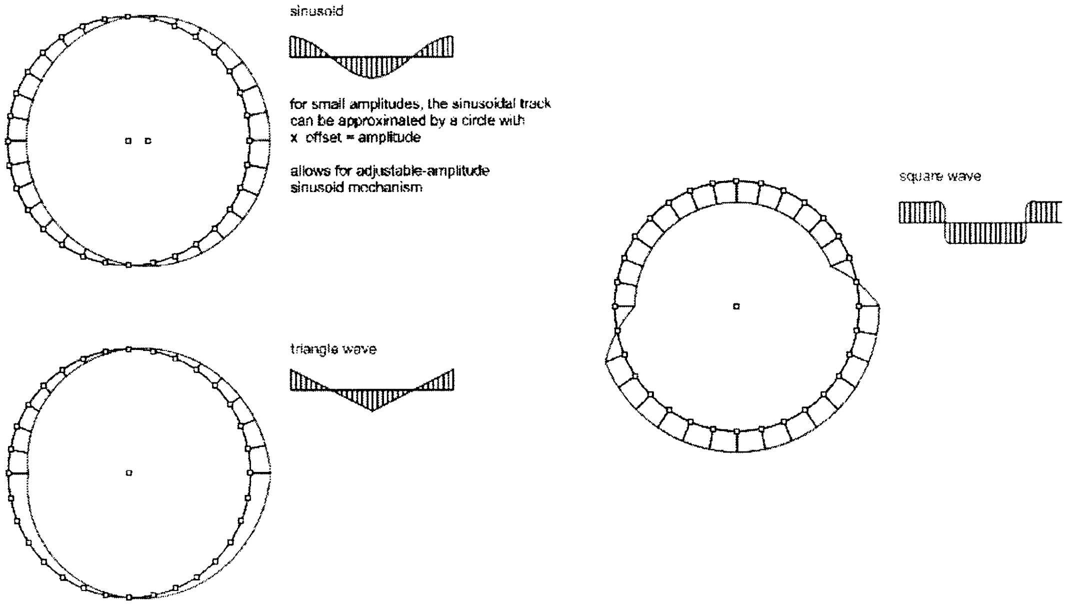
sinusoid
triangle wave
square wave

for small amplitudes, the sinusoidal track can be approximated by a circle with x offset = amplitude

allows for adjustable-amplitude sinusoid mechanism

Figure 3-12: Some interchangeable cams that would allow various wave shapes for the ring-shaped periodic robosnail 1.

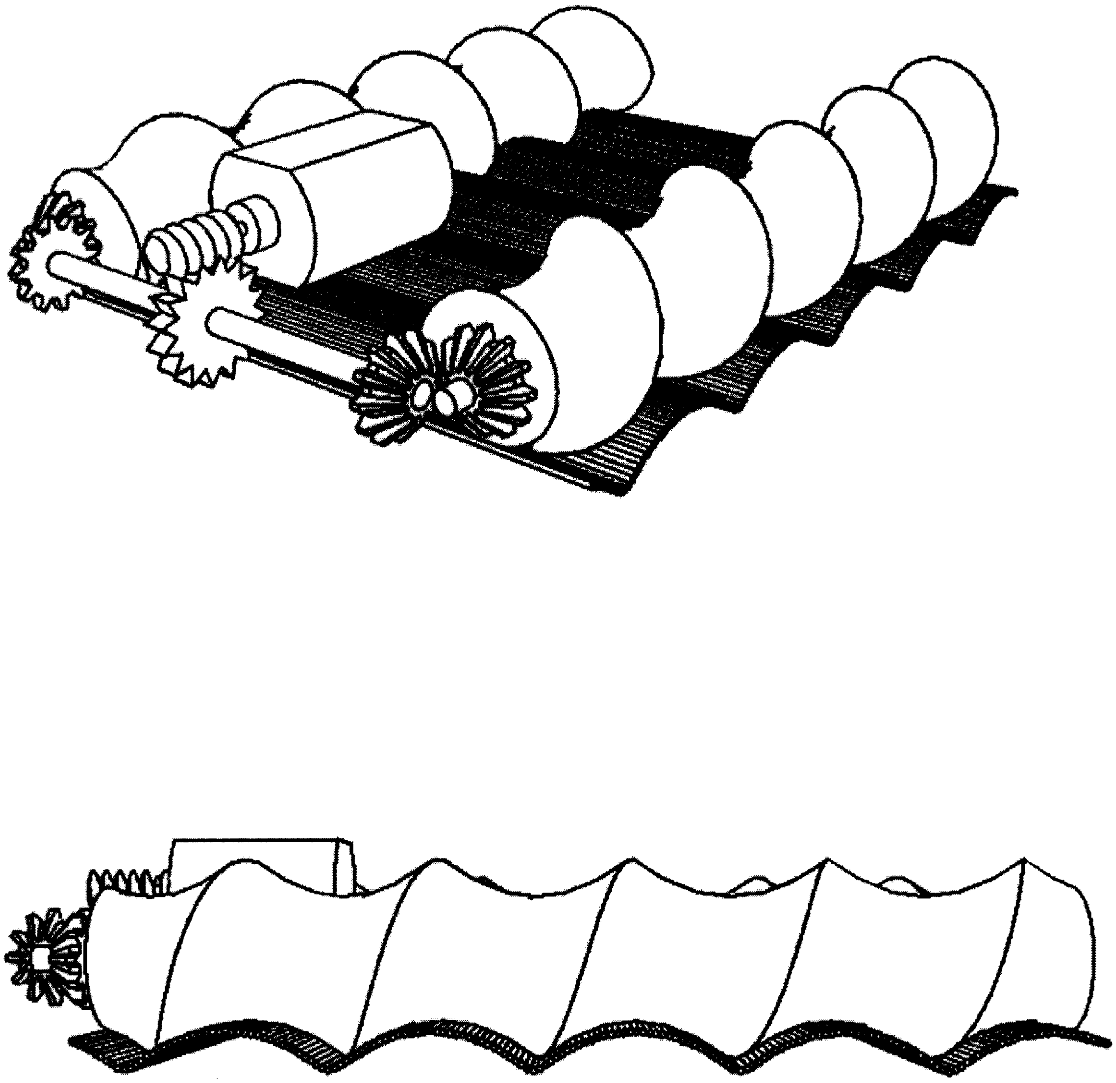

Figure 3-13: Another robosnail 1 type design for generating a non-sinusoidal waveform in the membrane. This particular design aims to test the "overdrive" phenomenon where the snail velocity exceeds its own waveform velocity. The membrane is reinforced with lateral stiffness members, and is stretched across two spiral cams. The rotational motion of the pair of spiral cams would transfer their translating profile to the membrane.

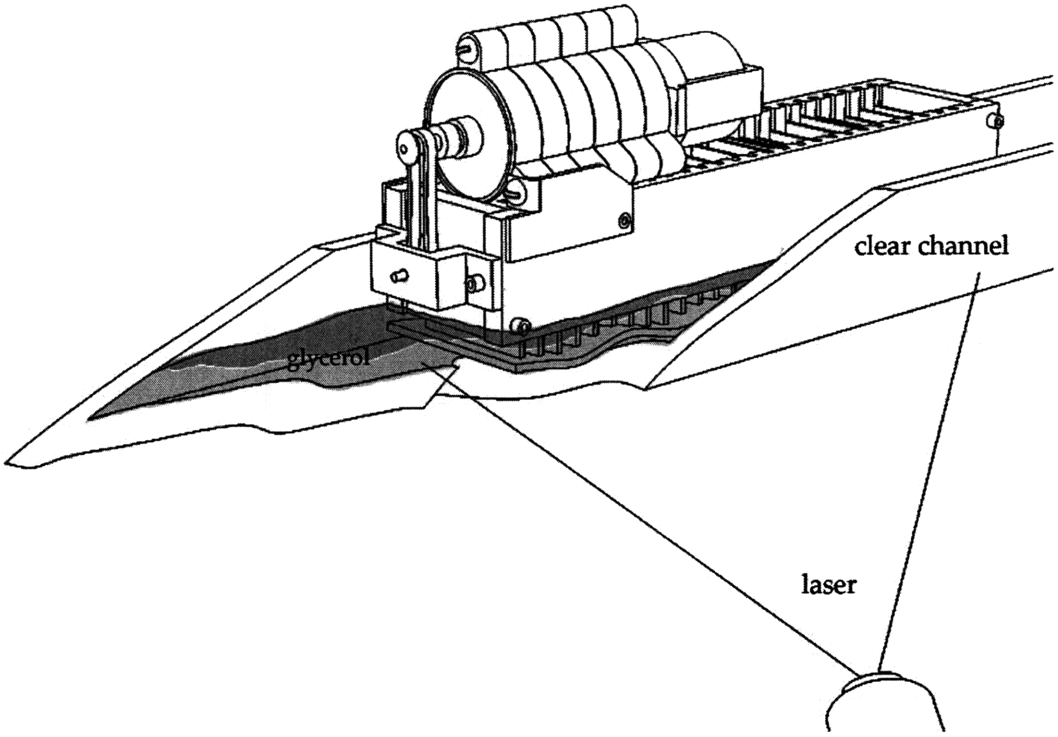

Figure 3-14: Set-up for measuring free velocity of robosnail. The channel contains the working fluid, enough to submerge the entire foot so that the peristaltic motion does not entrain air bubbles during operation. A laser sheet is shone at an angle onto the bottom foot surface, so that the profile could be measured and the wave profile and fluid thickness determined.

3.4 Experiment

Several experiments were conducted to test the analytical and numerical predictions. As we have seen already, differing wave shapes result in different forces and velocities, and conceivably a host of foot shapes could be experimentally analyzed. Due to the difficulty of constructing a device to generate custom waveforms, we only collected data for the sinusoidally waving robosnail.

The first experiment tested the free velocity of the snail without pulling any load. The snail was run in a pan of glycerol for some tests, later switching to silicone oil (the tendency of glycerol to absorb water from the air varied its viscosity from day to day, introducing experimental errors). The snail was first tested without any support – it was allowed to sink freely into the liquid, then the free velocity was measured as the foot neared the substrate. In later experiments the snail was placed on a track which held the snail at a constant

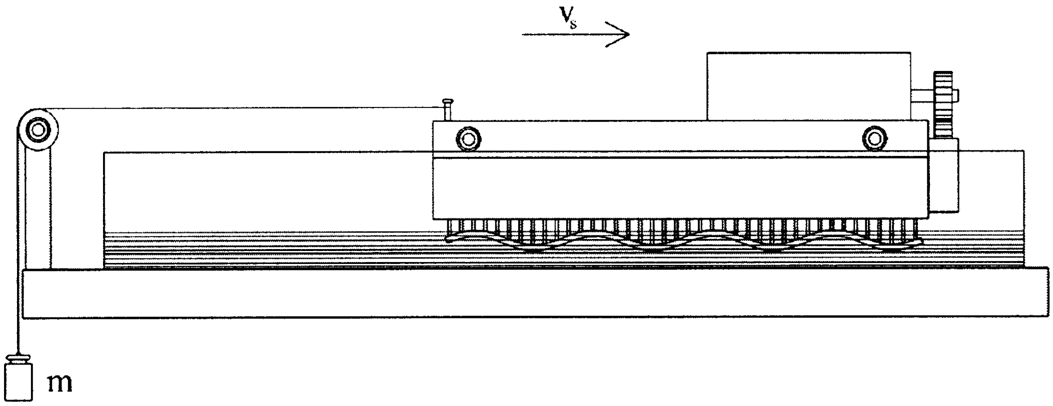

Figure 3-15: Set-up for measuring the moving tractoring force of the snail. Small support wheels on tracks hold the snail at a fixed height from the substrate, while the pulley setup allows the payload to be easily adjusted.

height from the substrate. Experiments also included a stationary force experiment to test the stall force of the waving robosnail at various heights and a moving force experiment (3-15), where various tractoring forces were applied to a waving robosnail, and the resultant velocity was measured.

3.5 Results and Discussion

It was found that the snail performed according to the predictions made by theory and numerical simulations. First, it was confirmed (figure 3-16) that the free snail velocity is proportional to the waving velocity when geometry and other variables were held constant. The 2D theory significantly over-predicts the constant of proportionality, consistent with the discussion on 3D effects.

The second test conducted was the stationary tractoring force, which we also expect to be proportional to the waving velocity. The data was consistent with the numerical results (figure 3-17).

The last set of data confirmed the linear tradeoff between tractoring force and waving velocity. The snail was operated at various waving speeds and the tractoring velocity was measured as it pulled loads of varying sizes. The load was increased and the tractoring force was found to drop linearly with velocity (3-18) as the theory predicted.

The last set of data describing the tractoring force varied slightly from the theoretical value in the slope of the force-velocity curve. The experiment found a greater tractoring

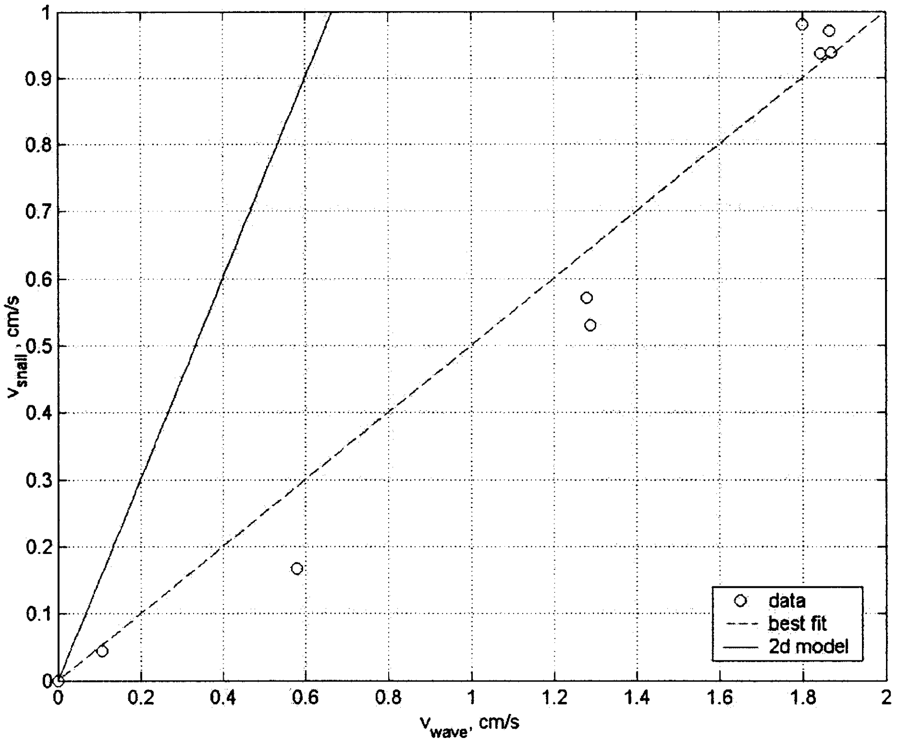

Figure 3-16: Free velocity of robosnail plotted against waving velocity. Fluid is silicone oil. The best-fit line coincides with the numerical result for a finite-width snail with dimensionless waving amplitude $a = 0.8$.

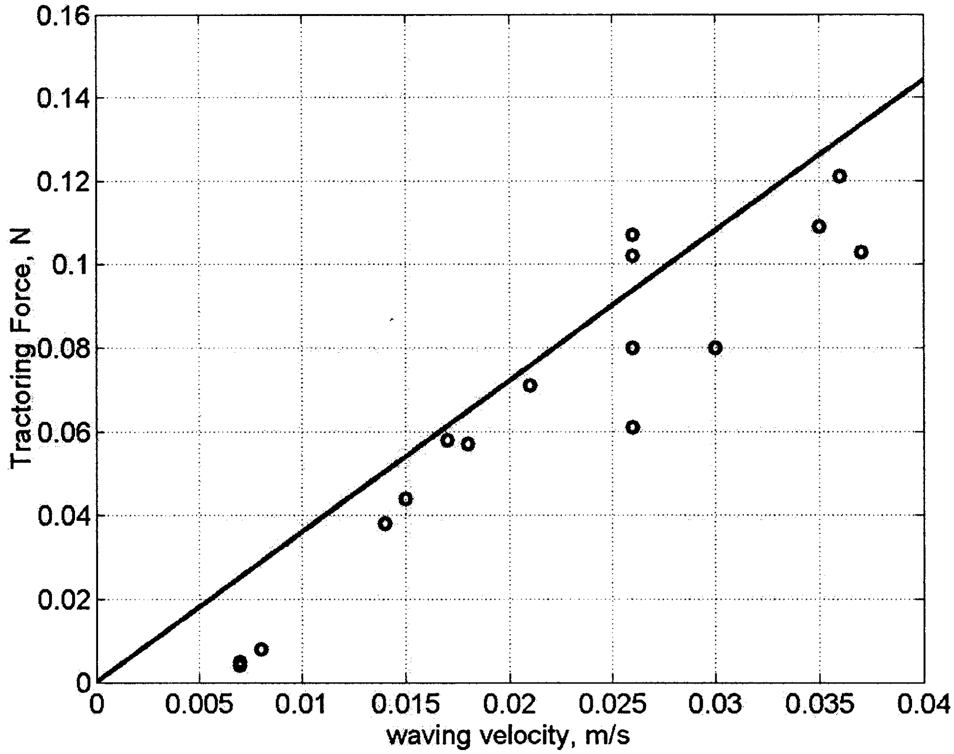

Figure 3-17: Tractoring force of Robosnail 1, plotted against waving velocity. The resultant tractoring force is linearly proportional with respect to waving velocity, as expected. The solid line represents the corresponding tractoring force predicted by numerical results for a snail of aspect ratio $b/l = 0.6$ with a sinusoidal wave amplitude ratio of $a/h = 0.7$. Fluid is silicone oil.

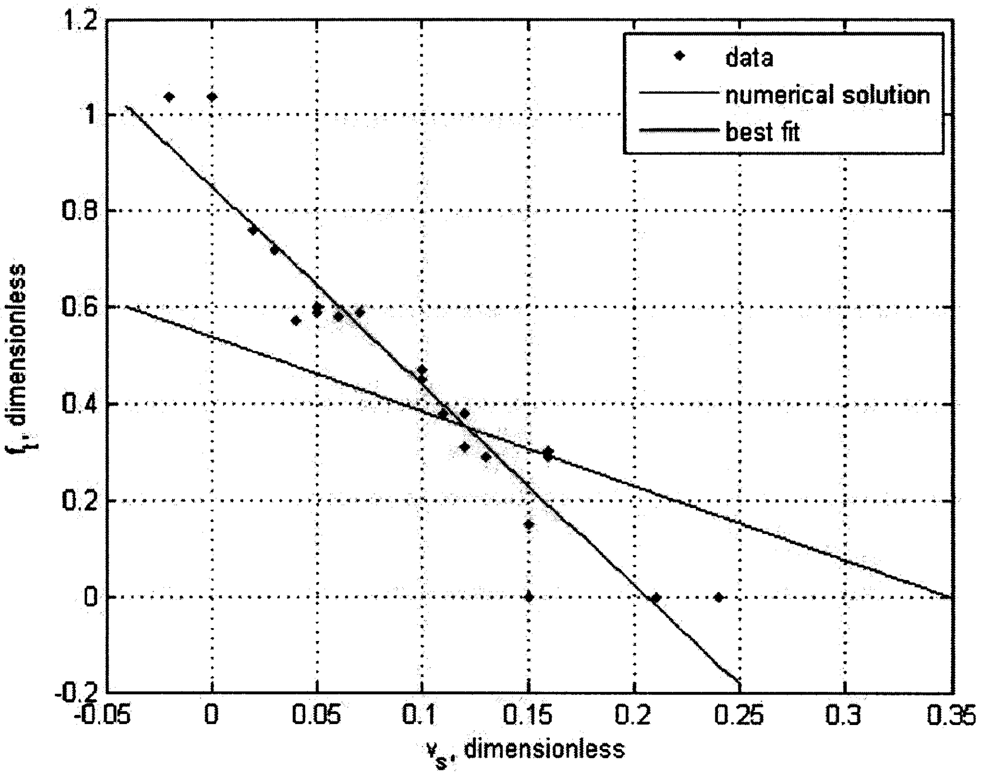

Figure 3-18: Force-velocity data for Robosnail 1. The payload force was increased while the robosnail velocity was measured. The snail velocity decreased linearly as expected. Fluid is silicone oil. The foot aspect ratio is aspect ratio $b/l = 0.6$, with a sinusoidal wave amplitude ratio of $a/h = 0.7$.

force for higher payloads, and a smaller tractoring velocity near the zero-payload free moving range. The most likely explanations for this discrepancy are that at low speeds, the fluid buildup behind the stalling robosnail resulted in an increase in hydrostatic pressure pushing on the snail in its favor. At high speeds, oil friction in the bearings probably caused the steeper drop-off in performance.

Chapter 4

Robosnail 2

4.1 Introduction

After producing Robosnail 1, we were motivated to develop a machine and fluid system capable of climbing walls and ceilings like live land snails (Robosnail 1 was only effective at moving over surfaces that were smooth and horizontal). With this goal in mind, we developed Robosnail 2. After reviewing several studies of land-snail locomotion [17, 18, 15, 16, 31, 32] and observing live snails in more detail, we found that most of the snails that were examined moved by adhesive locomotion, where propulsive forces are generated through fluid shear, rather than by pressure forces as in the case of Robosnail 1.

While Robosnail 1 is capable of moving through viscous fluids, it possesses several limitations. Real snails are known for their ability to traverse vertical and inverted planes, highlighting an important feature of snail mucus – finite yield stress. Robosnail 1, which is designed to run on Newtonian liquids, cannot climb walls unless it is completely submerged, as a Newtonian fluid would flow down and out of the gap by the force of gravity. Even if the device were submerged in a viscous fluid, a Robosnail 1 robot would require some sort of active pumping mechanism to keep itself adhered to the wall using fluid pressure, while real snails can adhere to a wall even when their foot is immobile. The benefits of Robosnail 2 mirror those of real snails in more ways than one: by using a non-Newtonian shear-stress fluid, Robosnail 2 can generate more force whether stationary or mobile, than Robosnail 1 (per unit of foot area) and was found to be more efficient than Robosnail 1.

Robosnail 2 will likely prove to be a useful proof-of-concept for later machines that operate in environments with non-Newtonian fluids. Mucus-filled cavities, oil drilling sites, lake bottoms, and other such environments are a few examples where snail-like adhesive locomotion might be advantageous.

4.2 Theory

At first glance, both Robosnails appear very similar: they are both mechanisms with a flexible foot, and they propel themselves over a thin lubrication layer of fluid using cyclical undulations of the foot. Despite these similarities, the two versions are fundamentally different. While Robosnail 1 relies on high lubrication pressures to propel itself, Robosnail 2 is propelled by the shear forces within the fluid film, and pressure forces are negligible. Furthermore, Robosnail 1 was built for use with a viscous Newtonian fluid, while Robosnail 2 requires a non-Newtonian fluid to move forward and, as we will show later, does not function with a Newtonian fluid at all.

The phenomenon of adhesive locomotion, as its name implies, is one of selective gluing and ungluing of an actuated membrane onto a substrate. In this illustration, the mucus acts as the glue. Unlike an ordinary glue, however, the mucus can be switched from solid to liquid states when subjected to a sufficient amount of shear force. This is essential in order that the snail be able to undergo a net motion. If the snail then generates traveling compression waves from one end of the membrane to another, such that the fluid beneath waves is sheared to the point of yielding, then the snail is able to travel forward incrementally with each new wave. As long as the fluid beneath the areas between sliding zones of the foot does not shear past the critical yield stress, the snail moves forward without slip. One final, necessary requirement of the fluid is that it be able to re-solidify (or restructure) after yielding; if this were not the case, the finite yield stress of the fluid would be lost after one motion cycle of the foot, and the snail would lose its ability to gain traction on the substrate.

4.2.1 Underlying physics

If we watch a snail moving beneath a piece of glass (figure 4-1), we can observe on the underside of the foot a distinct pattern of stripes. Close inspection of these moving stripes reveal them to be alternating zones of compression and expansion, which Denny [16] terms waves and interwaves, respectively. The compressed waves are moving forward from the

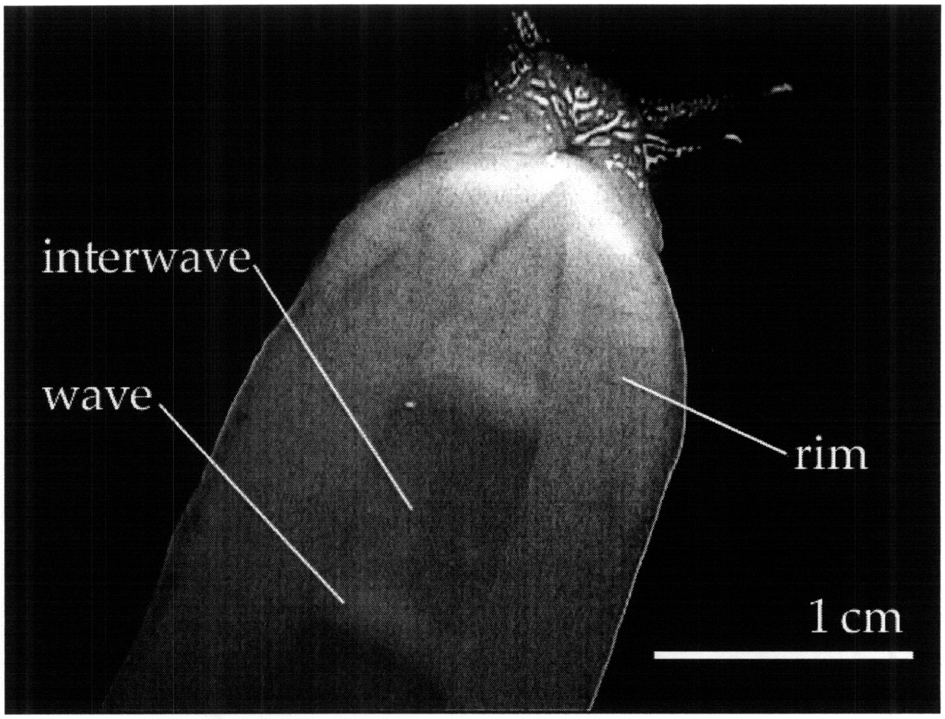

Figure 4-1: The underside of a moving slug (*Limax maximus*). The foot is divided into several regions; the interwave, which has material points stationary with respect to the glass surface, the waves, which are sliding forward with respect to the glass, and the rim, which is sliding at a constant velocity with respect to the glass. This study will focus on the wave and interwave regions.

tail to the head of the snail (direct waves). Certain marine snails [31] generate expansion waves instead of compression waves while moving; in this case, the waves move backwards (retrograde waves). In either case, the surface of a foot region within the wave is found to be sliding forward with respect to the ground, while the surface of an interwave is stationary with respect to the ground. The wave can be thought as a moving kink on a carpet, where the whole carpet represents the foot of the snail. By sliding the kink from one end of the carpet, one can move the carpet forward by an incremental amount. The direct waves must logically be compression waves since they resemble a standard carpet kink, in which material is bunched together; conversely, it follows that retrograde waves must be expansion waves (figure 4-2). A graphical space-time representation (figure 4-3) of the moving foot demonstrates how the relative sizes and speeds of the waves and interwaves are related.

A snail of this type has a flat foot, with a mucus layer of fixed height, whose surface

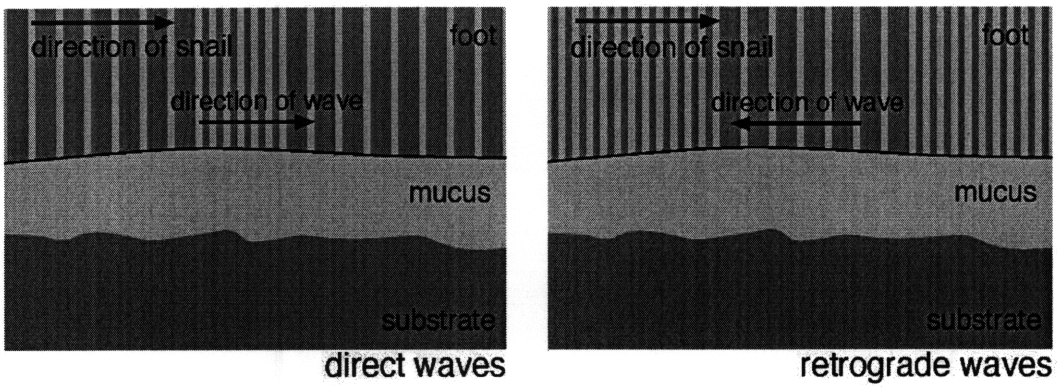
direction of snail
direction of wave
foot
mucus
substrate
direct waves
direction of snail
direction of wave
foot
mucus
substrate
retrograde waves

Figure 4-2: Snails moving with adhesive locomotion may apply direct or retrograde waves. The vertical stripes represent the relative local compression of the foot surface. Direct waves are necessarily waves of compression, while retrograde waves are necessarily waves of expansion

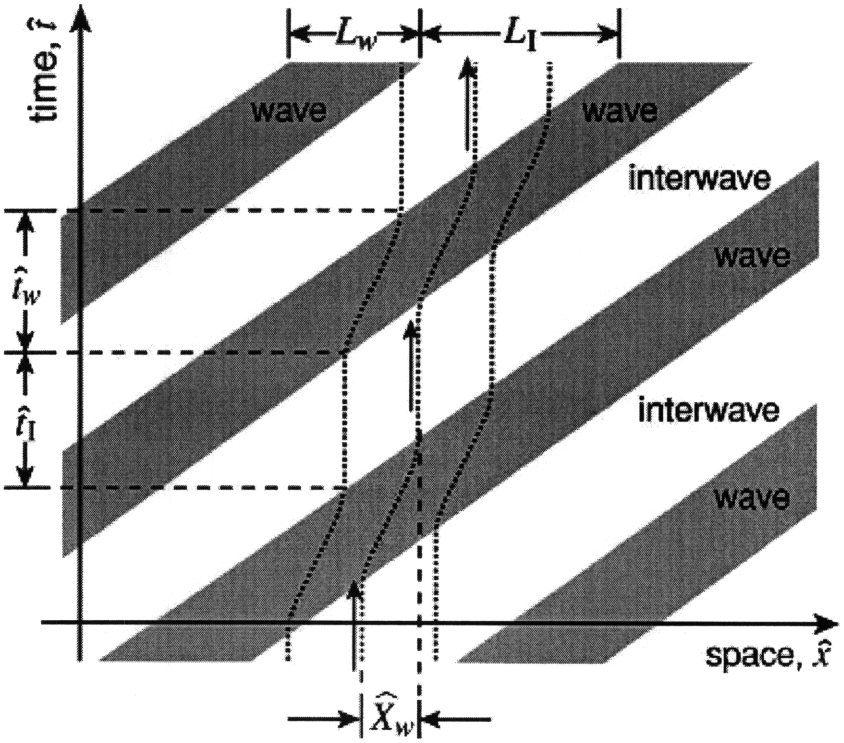
time, $\hat{t}$
L_W
L_I
wave
wave
interwave
wave
interwave
wave
$\hat{t}_W$
$\hat{t}_I$
space, $\hat{x}$
$\hat{X}_W$

Figure 4-3: A space-time representation of the waves and interwaves of the foot of a moving snail (from [10]). As the waves and interwaves move forward at a given velocity, the actual material points of the foot (given by the dotted line) move at a different velocity: while the point is within the interwave, it is stationary even though the interwave moves forward; while the point is within the wave, it moves faster than the velocity of the wave zones. L_W and L_I are the wave velocities, respectively, and $\hat{t}_w$ $\hat{t}_i$ are the times a material point remains within a wave and interwave, respectively. $\hat{X}_W$ is the increment of distance that the snail travels during the passage of a single wave.

deforms with a time-dependent displacement

$$\hat{u} = \hat{u}_x(\hat{x}, t),$$

where $\hat{x}$ is the dimensional distance along the x-axis and the deformation $\hat{u}$ is the displacement of a point on the foot from its average position. For our purposes, $\hat{u}$ is constrained to the horizontal plane in the $x-$ direction. We limit our analysis to traveling waves of a fixed shape

$$\hat{u} = \hat{u}(\hat{x} - \hat{V}_w t), \tag{4.1}$$

which are periodic such that

$$\hat{u}(\hat{x}) = \hat{u}(\hat{x} + \lambda),$$

and defined such that the average deformation is zero:

$$\int_0^\lambda \hat{u} d\hat{x} = 0.$$

At this point it is important to know the strain in the foot

$$\epsilon = \frac{\partial \hat{u}}{\partial \hat{x}}.$$

which in turn gives us the foot compression ratio

$$\frac{dx'}{d\hat{x}} = 1 + \frac{\partial \hat{u}}{\partial \hat{x}}$$

where x' is the new, deformed position of a point the foot at any given $\hat{x}$. The snail itself is moving at a velocity $\hat{V}_s$ so that the net velocity of a point is the sum

$$\hat{V}_p = \dot{\hat{u}} + \hat{V}_s.$$

Applying 4.1,

$$\hat{V}_p = \hat{V}_w \frac{d\hat{u}}{d\hat{x}} + \hat{V}_s.$$

The net force on the foot is equal to the tractoring force, and is the integral of all the shear forces on the foot,

$$\hat{F}_t = \int \tau dA.$$

For a snail of width b and length λ,

$$\hat{F}_t = b \int_0^\lambda \tau \left(1 + \frac{\partial \hat{u}}{\partial x}\right) dx. \tag{4.2}$$

If the fluid has viscosity μ,

$$\hat{F}_t = b \int_0^\lambda \mu \frac{\hat{V}_p}{h} \left(1 + \frac{\partial \hat{u}}{\partial x}\right) dx = b \int_0^\lambda \mu \frac{\hat{V}_w \frac{d\hat{u}}{dx} + \hat{V}_s}{h} \left(1 + \frac{\partial \hat{u}}{\partial x}\right) dx \tag{4.3}$$

Equations (??) and (4.3) describe the force-velocity relationship for any snail using in-plane foot deformations to move on a thin layer of fluid. Both (??) and (4.3) carry several conditions that we assume to be valid: first, that the pressure gradient $\frac{dp}{dx}$ is negligible and therefore that the velocity profile in the fluid gap is linear. For these conditions to hold for an incompressible fluid, we must assume that the foot height h would change slightly with x in order that fluid mass be conserved. However, we will assume that this change in h is small. Finally, the flow and the snail motion are assumed to be steady-state. The viscosity μ in this case is understood to be variable. In most cases described herein, viscosity is a function of shear rate $\dot{\gamma} = \frac{dv_x}{dy}$ but can vary according to other factors depending on the type of fluid used. It can be shown[1] when a Newtonian fluid is used, in-plane foot motions

---

[1] When this is the case, equation 4.3 becomes

$$\hat{F}_t = \frac{\mu b}{h} \int_0^\lambda \left(\hat{V}_w \frac{d\hat{u}}{dx} + \hat{V}_s\right) \left(\frac{\partial \hat{u}}{\partial x} + 1\right) dx$$

$$\hat{F}_t = \frac{\mu b}{h} \int_0^\lambda \left[\hat{V}_w \left(\frac{d\hat{u}}{dx}\right)^2 + \left(\hat{V}_w + \hat{V}_s\right) \frac{d\hat{u}}{dx} + \hat{V}_s\right] dx$$

$$\hat{F}_t = \frac{\mu b}{h} \left[\int_0^\lambda \hat{V}_w \left(\frac{d\hat{u}}{dx}\right)^2 dx + \int_0^\lambda \left(\hat{V}_w + \hat{V}_s\right) \frac{d\hat{u}}{dx} dx + \int_0^\lambda \hat{V}_s dx\right]$$

$$\hat{F}_t = \frac{\mu b}{h} \left[\hat{V}_w \int_0^\lambda \left(\frac{d\hat{u}}{dx}\right)^2 dx + \left(\hat{V}_w + \hat{V}_s\right) u|_0^\lambda + \lambda \hat{V}_s\right]$$

since the deformation is periodic, $\hat{u}(\lambda) = \hat{u}(0)$, the second term within the brackets goes to zero

$$\hat{F}_t = \frac{\mu b}{h} \left[\hat{V}_w \int_0^\lambda \left(\frac{d\hat{u}}{dx}\right)^2 dx + \lambda \hat{V}_s\right].$$

However, for small strains of the foot $\frac{d\hat{u}}{dx}$, $\left(\frac{d\hat{u}}{dx}\right)^2$ is small and the remaining integral is negligible. The remaining result

$$\hat{F}_t = \frac{\mu b}{h} \lambda \hat{V}_s$$

is independent of waving speed, and is only the viscous drag one would expect from dragging a membrane

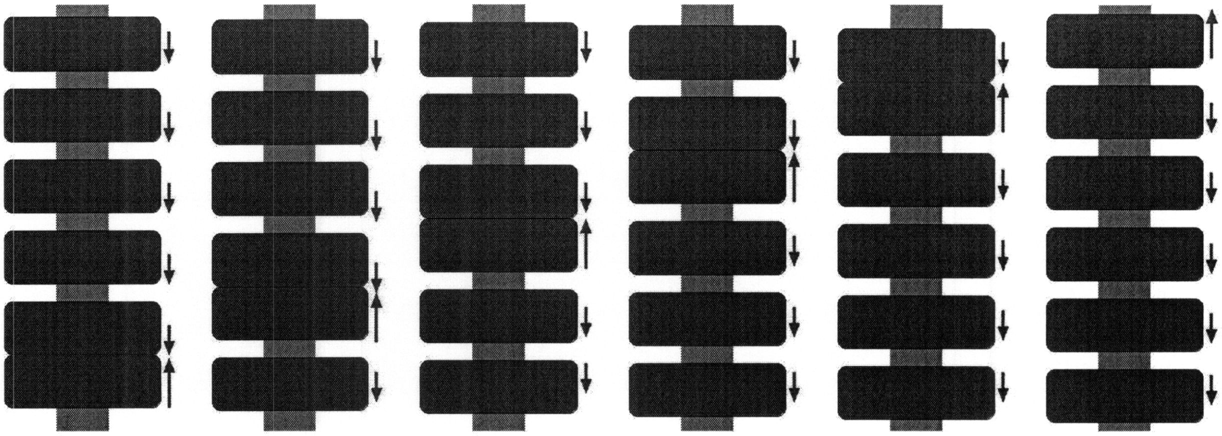

Figure 4-4: The motion sequence of a discretized Robosnail using direct waves to move upwards. The wave segment is the single faster-moving segment, while the remaining segments are the interwave.

cannot create a propulsive force; therefore, a non-Newtonian fluid is required for robosnail 2 to function.

To simplify the theoretical problem and the mechanical solution, we consider a snail composed of a foot divided into discrete sections (figure 4-4) which can each be considered uniform. We assume that the waves and interwaves are respectively of area A_w and A_i and move at steady velocities V_w and V_i. The net force integral can then be calculated as a product of shear stresses and their corresponding areas. Besides simplifying the analysis, this model can be achieved mechanically by constructing a foot consisting of n segments, and to employ a sliding pattern in which only $\frac{1}{n}$ of the sections is moving at $\hat{V}_w$ while the remaining segments move at $-\hat{V}_i$.

We use a force balance to analyze the snail locomotion in steady state. The forces on each of the foot segments are :

$$F_i = A_i\tau_i = A_i\mu_i\dot{\gamma_i}$$

$$F_w = A_w\tau_w = A_w\mu_w\dot{\gamma_w}$$

for the thin, constant thickness layer,

$$F_i = A_i\mu_i\frac{\hat{V}_i - \hat{V}_s}{h_0}$$

---

through a viscous fluid.

$$F_w = A_w \mu_w \frac{\hat{V}_w - \hat{V}_s}{h_0}.$$

Because the waving motion is prescribed by the mechanism design, the wave and interwave velocities $\hat{V}_w$ and $\hat{V}_i$ are measured with respect to the snail while $\hat{V}_s$ is measured in the lab frame. The sum of forces equal the tractoring force in steady state,

$$F_i + F_w = F_t.$$

The average velocity of any segment must equal zero with respect to the snail, $\frac{1}{\lambda}\int_0^\lambda \hat{V} dx = 0$ which results in $\hat{V}_i = -\frac{\hat{V}_w}{N-1}$, therefore

$$F_t = \frac{A}{N h_0}[\hat{V}_w(\mu_i - \mu_w) - \hat{V}_s(\mu_i(N-1) + \mu_w)].$$

This is the general equation for tractoring force given a Robosnail 2 mechanism configuration (N discrete pads moving with wave and interwave speeds). The result tells us that movement of the pads cannot generate thrust when the viscosity of the fluid is constant; if a Newtonian fluid is used, the only force that occurs is viscous friction if the snail is being dragged. The viscosity of the fluid in the interwave must be greater than the fluid in the wave for the foot motion to create any positive tractoring force, and this is the case with real snails. We can conclude from this result that the thrust is forward for a shear-thinning fluid, and backward for a shear-thickening fluid, where the viscosity in the slow interwave would be less than that in the faster moving wave.

It can be shown[2] that for the discrete interwave/wave model with described above, the foot cannot apply a net force on the substrate if the gap is filled with a Newtonian fluid. If,

---

[2] When this is the case, the fast moving smaller section experiences a force of

$$F_w = \mu \frac{A(\hat{V}_w - \hat{V}_t)}{N h_0}.$$

The slow moving interwave section feels an opposing force of

$$F_i = \mu \frac{A(N-1)(-\hat{V}_i + \hat{V}_t)}{N h_0} = \mu \frac{A(N-1)(-\hat{V}_w/(N-1) - \hat{V}_t(N-1))}{N h_0}.$$

The total fluid force exerted on the snail is then

$$F = \mu \frac{A(\hat{V}_w - \hat{V}_t) + A(-\hat{V}_w - \hat{V}_t(N-1))}{N h_0} = -\mu \frac{A\hat{V}_t}{h_0}.$$

When we consider the a snail without tractoring force, the forces from foot motion exactly balance, and the net force is due to the relative motion of the snail, $\hat{V}_t$. The snail will drift with a constant velocity, (as if it were a rigid plate dragged through a viscous Newtonian fluid) independent of $\hat{V}_w$.

however, the fluid is a Bingham fluid (or any fluid that exhibits a shear stress that is not linear with shear rate), the behavior is different. In the following model we assume that the fluid has not yielded underneath the interwave (a condition we are trying to maintain).

The tractoring force and resultant speed of the snail are highly dependent on the viscosity function of the fluid, and many results can be found using different types of non-Newtonian fluids. It is important to keep in mind that the viscosity of non-Newtonian fluids depends on the shearing rate itself, therefore evaluating the force equation is often nontrivial. The Bingham fluid approximation provides certain simplifications that yield a useful analytic result.

4.2.2 Bingham fluid approximation

One practical non-Newtonian fluid is the Bingham fluid [7, 37, 38], which is similar to Newtonian fluids in that the stress increases proportionally with strain rate, the only difference being that a certain yield stress needs to be exceeded before the fluid starts to flow. Many clays can behave like Bingham fluids and are well approximated by the model. We can apply a similar force-balance analysis as shown above using a Bingham fluid as lubricant.

We assume a Bingham fluid model for the non-Newtonian fluid filling the gap of uniform thickness h_0. The total contact area is A, divided into N discrete sections. Recall from the Robosnail 2 model that at all times, $\frac{1}{N}$ of the area of the foot is moving upward with a speed of $\hat{V}_w$ while the rest of the $\frac{N-1}{N}$ segments are moving downward with a speed of $\frac{-\hat{V}_w}{N-1}$. We will refer to these two areas of the foot the wave and interwave, respectively. With respect to the substrate, the wave moves forwards at $\hat{V}_w - \hat{V}_t$ and the interwave moves backwards with $\frac{-\hat{V}_w}{N-1} - \hat{V}_t$. (Note that we desire $\hat{V}_t$ to be negative.

The Bingham number is defined as

$$B = \frac{\tau_y h_0}{\mu \hat{V}_w}, \tag{4.4}$$

which is the ratio between the yield stress and the Newtonian fluid stress in the fluid. Essentially, a larger Bingham number corresponds to a greater deviation from Newtonian behavior, where the limit of $B = 0$ corresponds to the zero yield stress of a Newtonian fluid. The stress under the interwave τ_i will be rewritten as:

$$\tau_i = \frac{1}{S}\tau_y,$$

where S is a the safety factor, defined such that $1/S$ is the fraction of the yield stress reached beneath the interwaves. For there to be no slip locomotion, we require $S > 1$. The force balance on the snail becomes as follows. On the wave, $F_w = (\tau_y + \frac{\mu(\hat{V}_w+\hat{V}_t)}{h_0})\frac{A}{N}$, while on the interwave, $F_i = \frac{1}{S}\tau_y\frac{N-1}{N}A$. The sum of the forces is

$$\hat{F}_t = F_w + F_i = \frac{A\tau_y}{N}(\frac{1}{S}(N-1) - \frac{1}{B}\frac{N}{N-1} - 1) \tag{4.5}$$

The maximum force the snail can sustain without slipping is the tractoring force when $\frac{1}{S} = 1$ and $\tau_i = \tau_y$. As long as the condition $\frac{1}{S} \leq 1$ holds, there is no slip and the interwave velocity with respect to the ground is zero,

$$\hat{V}_i - \hat{V}_t = \frac{-\hat{V}_w}{N-1} - \hat{V}_t = 0,$$

and the tractoring velocity can be deduced:

$$\hat{V}_s = \hat{V}_i = -\frac{\hat{V}_w}{N-1}$$

.

4.2.3 Motion with slippage

Once τ_i increases beyond τ_y, the foot slips, and the forces in the wave and interwave are both functions of the yield stress and the tangent viscosity:

$$F_w = \frac{A}{N}(\tau_y + \mu\frac{\hat{V}_w + \hat{V}_s}{h_0})$$

$$F_i = \frac{(N-1)A}{N}(\tau_y + \mu\frac{\frac{\hat{V}_w}{(N-1)} - \hat{V}_s}{h_0}),$$

defining $V_s = \frac{\hat{V}_s}{\hat{V}_w}$ the force balance with slippage becomes

$$\hat{F}_t = \frac{A}{N}\tau_y[N - 2 - \frac{NV_s}{B}],$$

which has a linear force-speed curve similar to Robosnail 1. Note that even with slippage, there can still be a net motion. For the sake of completeness, there are three more states of slip and non-slip motion of the snail. These regimes involve the presence of slipping and non slipping regions and depend on the Bingham number, the number of pads N, and the fluid viscosity and yield stress (Figure 4-5).

Each of the force-velocity relations for the individual regimes can be solved by a force balance. When a high enough load is applied, the snail will experience back-slip in both the wave and interwave areas. The force-velocity relation for this case is

$$F_t = \frac{\hat{F}_t H}{A\mu \hat{V}_w} = -V_s + B;, \qquad \mathit{for} \qquad v_t < -1. \tag{4.6}$$

Eventually the force is small enough that the forward-sliding wave region feels a stress less than the yield stress of the fluid, and does not slide relative to the substrate. Since the wave is moving forward (relative to the snail) with a velocity of $\hat{V}_w$, the snail is moving backwards at a velocity of $-\hat{V}_w$. This configuration remains stable as long as the absolute value of the stress within the wave is less than the yield stress, $-\tau_y < \tau_w < \tau_y$. As the applied force is decreased more, the relative force of the interwave is enough to overcome the yield stress of the wave area, and the wave begins to slip forward while the interwave is still slipping backwards. The force-velocity function becomes:

$$F_t = -V_s + B\frac{N-2}{N}, \qquad \mathit{for} \qquad -1 < v_t < \frac{1}{N-1}. \tag{4.7}$$

As the applied force is decreased even more, the fluid beneath the interwave ceases to yield, and the snail travels forward at the intended design velocity $\hat{V}_s = \hat{V}_i$. This is a stable configuration as long as the interwave fluid has not yielded $-\tau_y < \tau_i < \tau_y$. Because of the relatively large interwave area, there exists a good range of tractoring forces in which the snail moves at the no-slip velocity. The snail will move at $\hat{V}_i$ even after the applied force becomes positive, pushing the snail forwards. Eventually, a great enough pushing force will yield the fluid beneath the interwave as well as the wave, and the snail will begin to slip forward:

$$F_t = -v_t - B, \qquad \mathit{for} \qquad \frac{1}{N-1} < v_t. \tag{4.8}$$

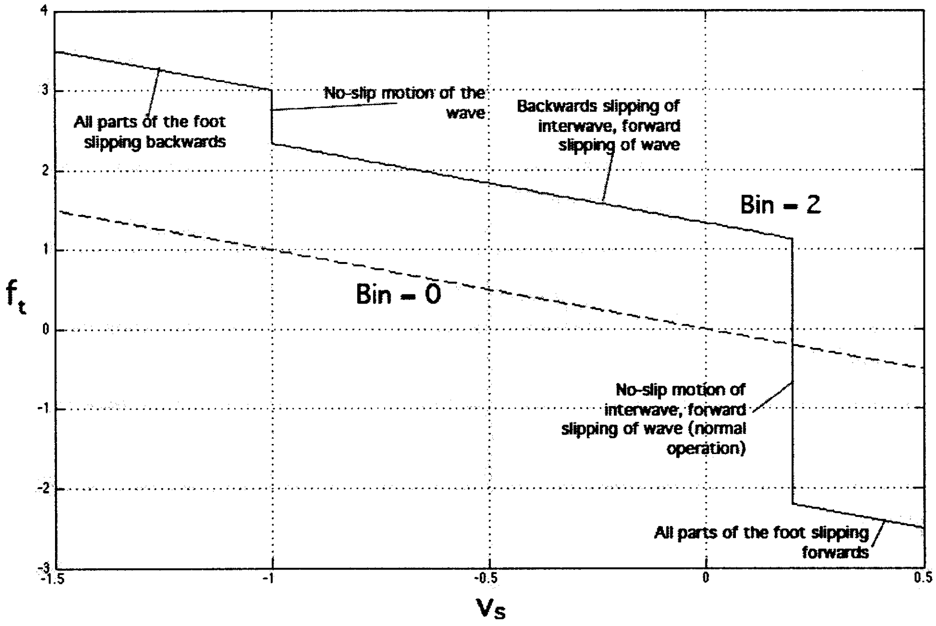

Figure 4-5: Tractoring force - velocity relationship for robosnail 2. The graph shows various regimes of motion for robosnail 2, depending on tractoring force. At one extreme (far left), the applied load is so great that both the snail slips backwards, and there is slippage beneath the wave and interwave regions. At the other extreme (far right), the applied load is positive, and pushes the snail such that there is slippage forwards, against fluid drag forces beneath the snail. Between these two extremes there is a range at which the foot motions can propel the snail forwards without slippage at a velocity $\hat{V}_i$. Note that with zero Bingham number, we are left with the strictly Newtonian case, wherein no force can be generated by waving foot motions.

Note that as the Bingham number goes to zero, the fluid yield stress is minimized and we are left with a tractoring force that is proportional to the slipping velocity (the Newtonian case where $\hat{V}_w$ has no effect).

4.2.4 Power and Efficiency

Once the force and velocity relations are well defined, finding the power requirement is straightforward. The total power consumed is the sum of the power required to move the interwave and the power required to move the wave,

$$\dot{W}_{in} = \sum_j F_j v_j = F_w \hat{V}_w + F_i \hat{V}_i,$$

while the useful power output is the product of the tractoring force and the tractoring velocity,

$$\dot{W}_{out} = \hat{V}_s \hat{F}_t,$$

and the efficiency is the ratio

$$\eta = \frac{\dot{W}_{in}}{\dot{W}_{out}}.$$

By substituting the equations for force and tractoring velocity, we arrive at the following expressions for the power and efficiency:

Without slip:

$$\dot{W}_{in} = \frac{A}{N}\tau_y V_w[1 + 1/S + \frac{1}{B}\frac{N}{N-1}]$$

$$\eta = \frac{1/S - \frac{N}{B(N-1)^2} - \frac{1}{N-1}}{1 + \frac{N}{B(N-1)} + 1/S}$$

With slip:

$$\dot{W}_{in} = \frac{A}{N}\tau_y V_w[2 + \frac{1}{B}\frac{N}{N-1}]$$

$$\eta = \frac{(N - 2 - \frac{Nv_t}{B})V_s}{2 + \frac{N}{B(N-1)}}.$$

Notice that as S approaches 1, the power and efficiency expressions of the no-slip case approach that of the slip case.

We can see that higher efficiencies are attained at higher Bingham numbers. This makes sense because high Bingham numbers represent a greater deviation between apparent viscosities of the working fluid, while at lower Bingham number, the setup resembles the Newtonian case, which we have already proven cannot generate a tractoring force and hence exhibits zero power output and efficiency. For each efficiency curve, the curve intercepts the x-axis at a nonzero $1/S$; this is the point at which the snail starts moving, and before which a forward F_t must be applied for the snail to be moving in the correct direction; the negative required input power results in a negative efficiency. The highest efficiency occurs when $S = 1$. Efficiency decreases quickly at higher $1/S$ since additional forces would be required to overcome viscous friction in the interwave region. Efficiency again falls to zero after a certain value of $1/S > 1$; this is where the interwave exerts just enough force to sustain the drag force of the wave.

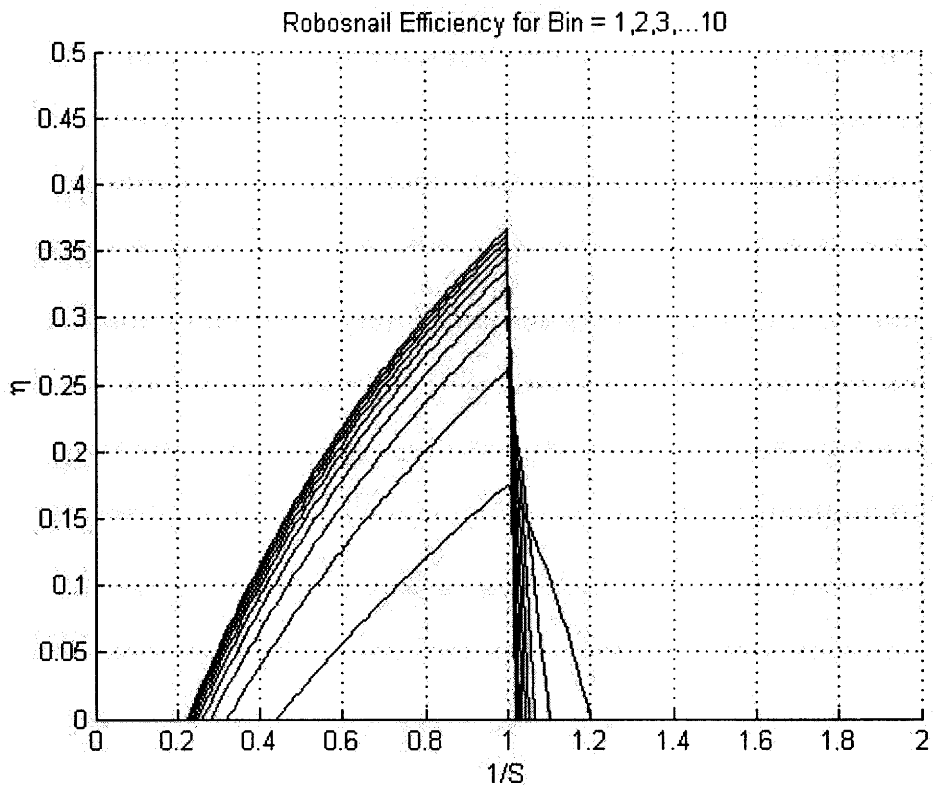

Figure 4-6: Tractoring efficiency for Robosnail 2, N = 6, varying the shear factor $1/S = \frac{\tau_i}{\tau_y}$. Curves shown for B = 1, 2, 3, ... , 10. The bottom curve is for $B = 1$.

4.2.5 Safety vs. efficiency

While it is favorable to maximize the efficiency of the snail, certain applications involving large scales and forces may require strict safeguards against the catastrophic breakdown of the fluid. This breakdown can theoretically occur for certain fluids such as Laponite that exhibit such high shear-thinning behavior that the shear stress decreases below the yield stress at higher shear rates [53, 1, 3]. Once the tractoring force is increased to the point where the interwave and wave have yielded, the force balance becomes unstable and the snail continues to slide backwards with increasing speed. Hence, while the use of highly shear-thinning fluids is favorable for maximizing efficiency (by decreasing the wave drag), Bingham fluids (with positive μ) may be favored for safer operation since a faster back-slip would be met with higher fluid resistance, limiting the speed of slippage to a stable value.

4.3 Mechanical Design

An early incarnation (figure 4-7) of Robosnail 2 employed N foot pads independently actuated by lengths of Nitinol "muscle wire". The prototype, which used an external power source, was lightweight enough to climb walls and move upside down using a thin layer of Laponite suspension. The shape memory wires are capable of a maximum strain of about 5%. To maximize the total displacement of the foot pads, the design used Nitinol wires spanning the entire length of the snail. The pulley assembly at the front of the snail allowed the wire tension to be transmitted to the corresponding foot pad. Because of their structure, the wires are only capable of exerting a tensile force upon activation, and require an outside source to re-extend. Each of the foot pads were fitted with return-springs in order to return the pad and the Nitinol wire to its initial position.

The complexity of the control, the slow restructuring time and low yield stress of the Laponite, and resultant small maximum size of Robosnail led us to continue development of an improved version. An intermediate idea to simplify the actuation of the foot was to incorporate a cylindrical rotating cam in which a series of grooves was carved (figure 4-8). The grooves were each composed of two spiral segments: one long segment spanning most of the circumference turning counterclockwise, and the second segment spanning the remainder of the circumference turning backwards clockwise, connecting the ends of the long groove. Each groove was identical to the next except for a fixed angular offset between

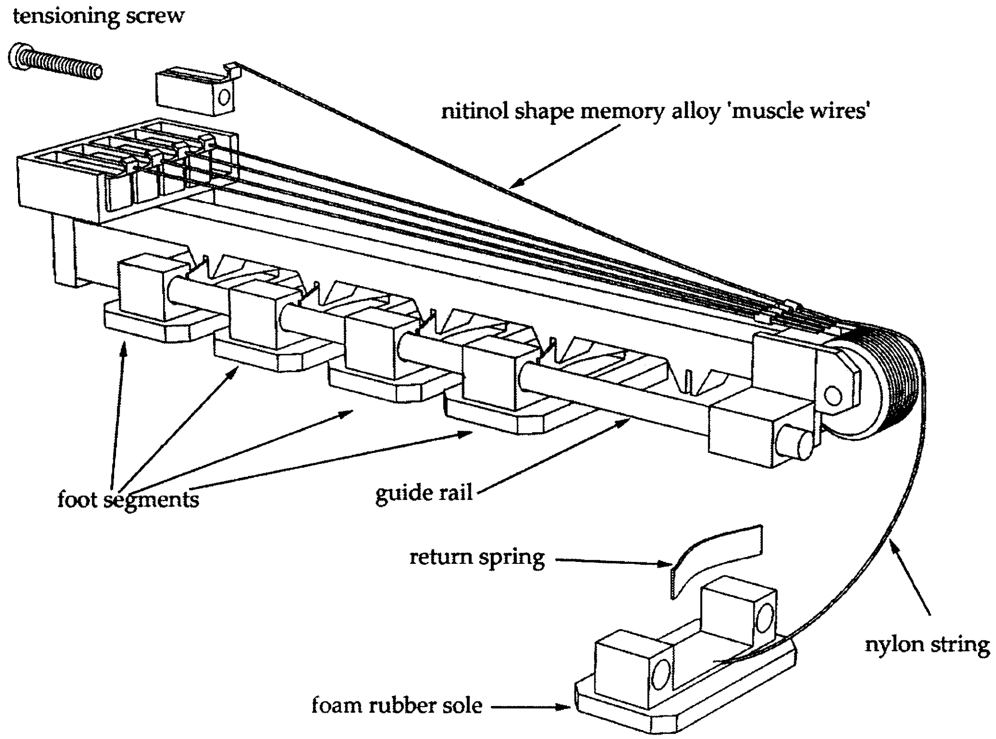
tensioning screw
nitinol shape memory alloy 'muscle wires'
foot segments
guide rail
return spring
nylon string
foam rubber sole

Figure 4-7: The first version of Robosnail 2 used shape-memory (Nitinol) wires to actuate the foot sections. This gave the advantage of compactness and minimized weight, but disadvantages were the slow and small movements of the segments (limited by the strain and cooling time required by the shape memory alloy) and the need for an umbilical cable.

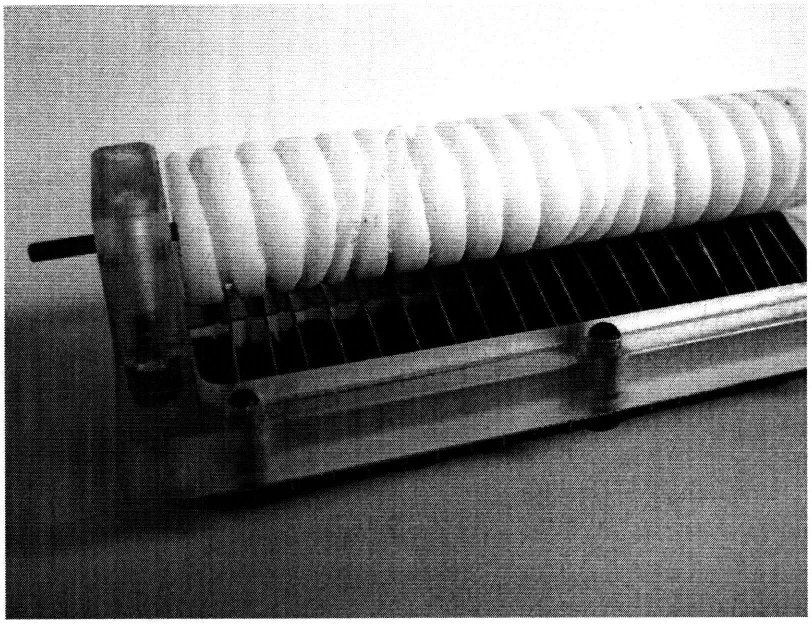

Figure 4-8: Adhesive robosnail using multiple cylindrical cams.

each groove. A foam rubber foot with perpendicularly embedded metal plates was mounted beneath and parallel to the rotating cylinder such that the edge of each plate rested within its own groove. Finally the metal plates were constrained by the frame to rotate about their midpoint. As the cam was rotated, each of the plates tilted according to the rotation of the groove, the net effect being a moving pattern of compression waves mimicking that of a live snail. While this transmission device solved the actuation problem, the large cylinder was too massive to allow wall climbing, and the cutting of the grooves was a costly process that hindered prototyping.

The cylinder cam mechanism was later simplified into a mechanism consisting of a single spiral groove cam (figure 4-9) with eight cam followers embedded in the groove at separate angular positions. The offset angular positions of the followers was a mechanically simpler solution than using a series of grooves and decreased prototyping difficulties as well as machine mass. Instead of a continuous, compressible membrane, rigid sections formed the foot. Each of the cam followers was connected to a foot segment. Since the mass of the mechanism was decreased, the snail was capable of traversing inclined surfaces up to 45 degrees, but was still too heavy to move vertically. The single cylinder cam had a geometry that could not be easily manufactured.

Further improvements led to the next version (figure 4-10) of Robosnail, which is powered by a single motor, carries its own battery pack, and operates on an aqueous solution of

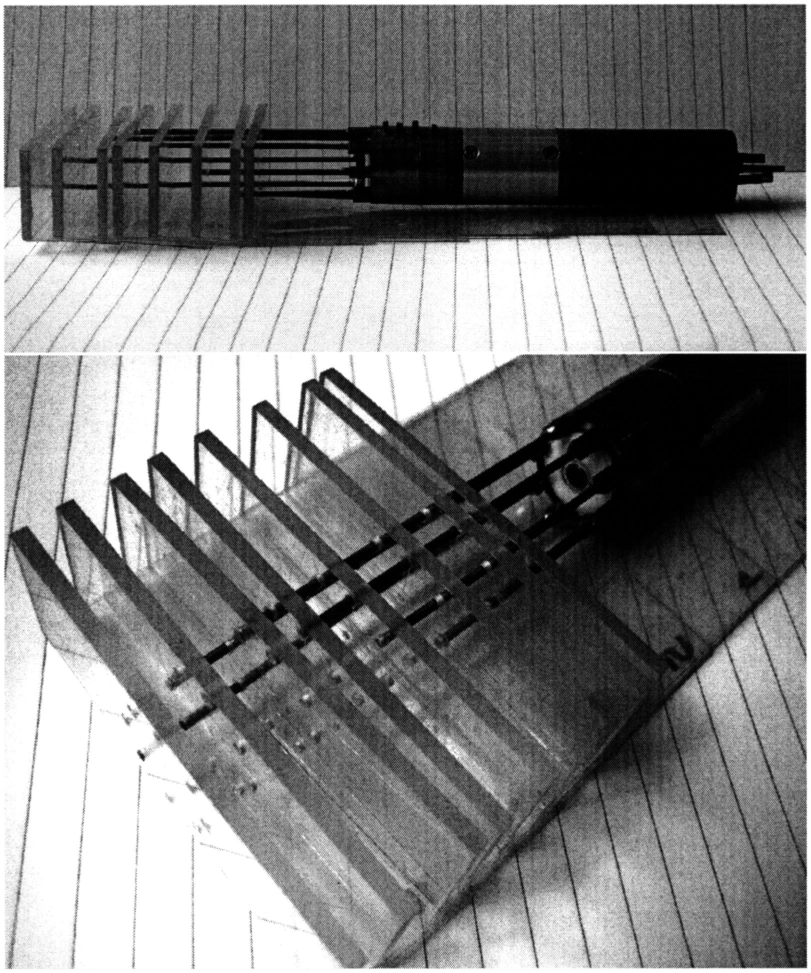

Figure 4-9: Adhesive robosnail using a single cylinder cam.

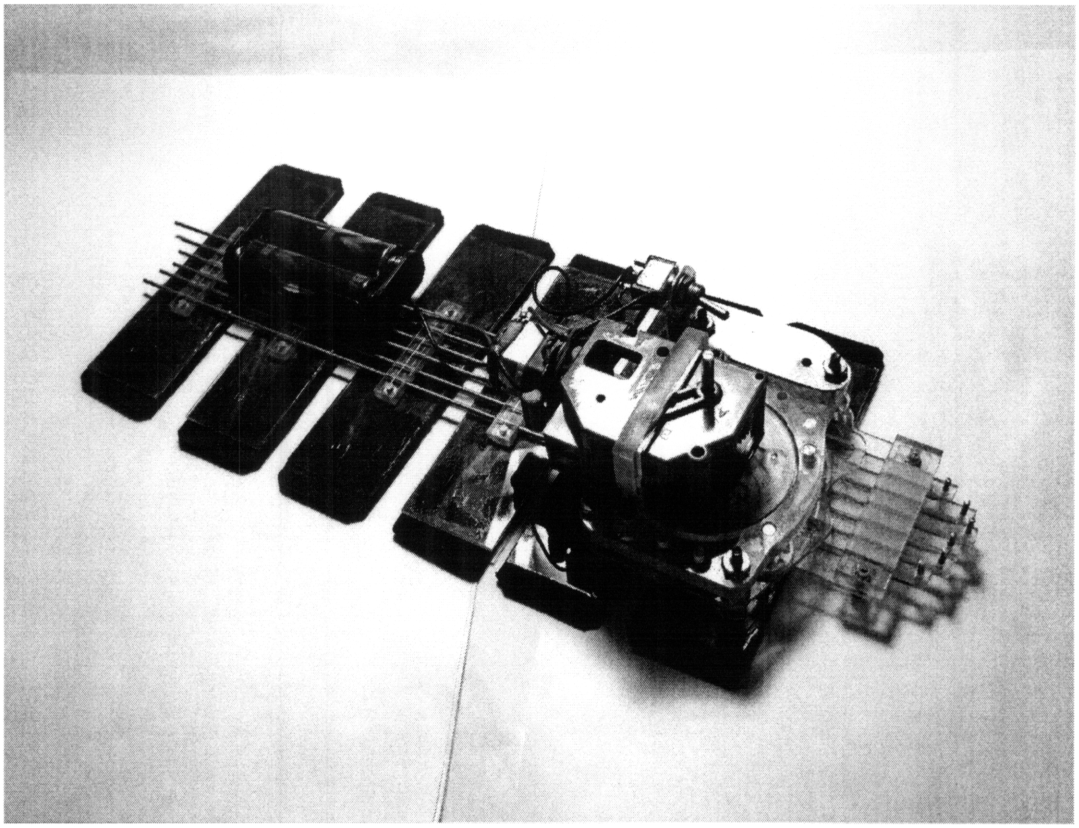

Figure 4-10: Robosnail 2nd generation.

Carbopol, a stronger yield-stress fluid with a faster restructuring time than Laponite. The higher power-to mass ratio of the new mechanism, coupled with the increased yield stress of the working fluid allowed us to build a larger, more robust prototype that was finally able to scale a vertical incline.

At the heart of Robosnail 2 is the newly developed transmission assembly (figures 4-11, 4-12) which gives the separate foot pads their motion. The transmission consists of a slowly rotating disk cam, which is powered by the geared-down motor, a set of six arms that follow the track, and linkages between the arms and the foot pads. By guiding the positions of the arm tips as it rotates, the track groove on the rotating disk defines the oscillatory motion of the foot pads. Because each of the guiding arms is located at an angle $\frac{360^\circ}{N}$ from the previous arm, each of the pads likewise is separated by the proper phase.

We recall from the theory that for N pads, we want one of the pads (at any instant, this would be the wave pad) to be moving forward with a speed of $\hat{V}_w$, while the remaining pads move backwards at $\hat{V}_i = \frac{\hat{V}_w}{N-1}$. The track shape that fits these requirements is composed of two segments of linear spirals, one steadily increasing radius over $\frac{N-1}{N}$ of the circle, and

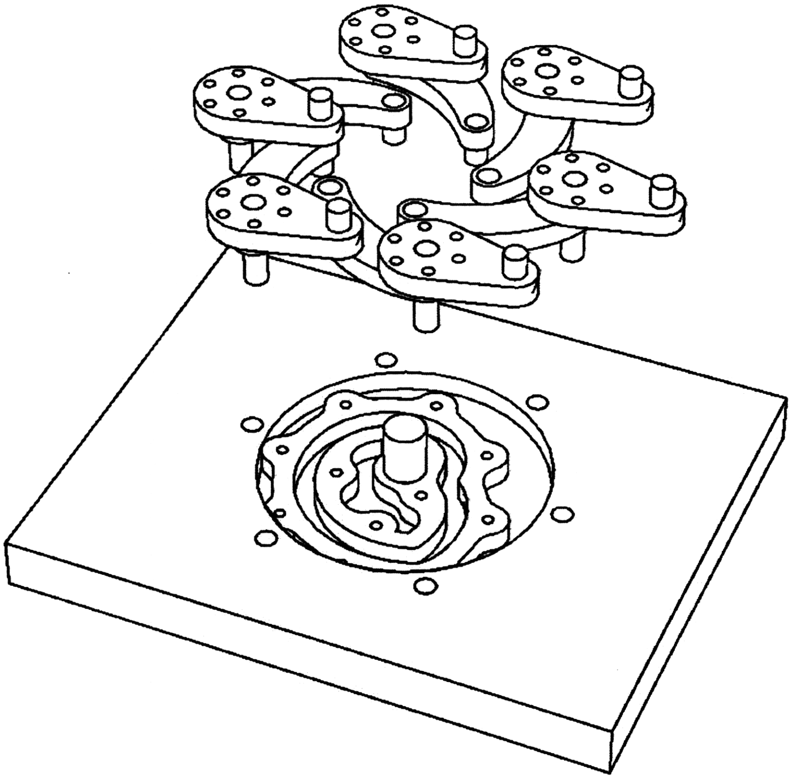

Figure 4-11: An exploded view of the internal transmission device of the second-generation Robosnail 2. The circular structure is the cam, surrounded by 6 followers. The followers each control one of the six foot segments in a linear motion.

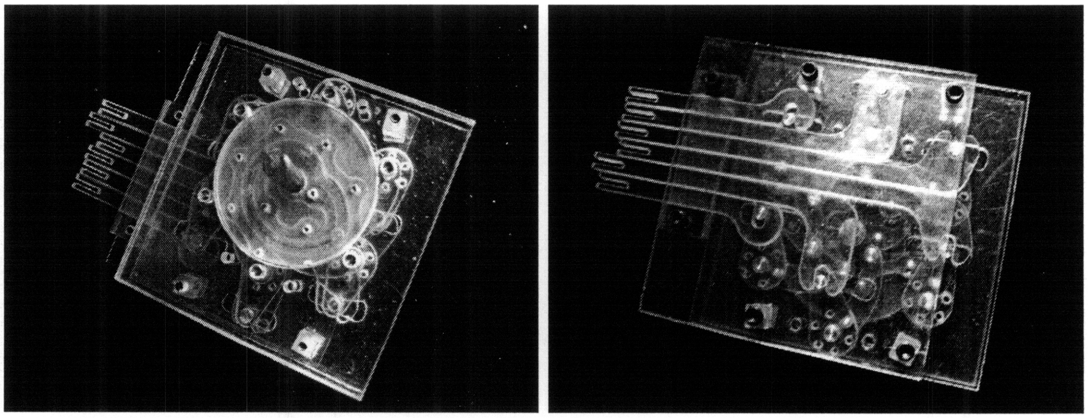

Figure 4-12: Top and bottom views of the cam device.

the other spiral connecting the ends of the long spiral over $\frac{1}{N}$ of the circle. The foot pads of Robosnail 2 are each mounted on a rigid linear guide, so they are constrained to slide forwards and backwards with minimal sideways deviation.

4.4 Experiment

The snail was run on a thin layer of fluid on various inclines. The fluid was first spread onto the surface in a layer that was constant in thickness; then the snail was manually adhered to the surface. The first snail was tested with a solution of Laponite, an aqueous suspension of synthetic clay. The second generation, motor-powered model was tested on solutions of Carbopol, a proprietary compound produced by the Lubrizol corporation. Figure 2-2 shows for a range of concentrations, the fluid has a noticeable shear-thinning behavior. The Carbopol solution has a much higher yield stress and so was able to support the bulkier snail when it was tested on higher angles of inclination.

4.5 Results and Discussion

As we expected, the snail velocity was maximal on a horizontally oriented plane relative to inverted or climbing vertically. The slowest results came from trying to move up a vertically inclined plane, with gravity pulling on the full weight of the snail. While inverted motion was not hindered by gravity in the direction of motion, one unforeseen problem was that gravity caused the snail to delaminate and peel away from the surface. Eventually the snail would delaminate to a point where the fluid could no longer support its weight, and the device would fall from the test surface. The first test, with the muscle wire snail operating on Laponite (figure 4-13), displayed the most forward motion at zero degrees (horizontal motion), and the least motion at around 90 degrees (vertical motion).

The second snail was capable of pulling a greater payload, and was able to attain a much higher velocity than its predecessor (figure 4-14). While Carbopol is not strictly a Bingham fluid, it can be approximated as such, and the fluid constants for the Bingham approximation of Carbopol at 7% concentration by weight are $\tau_y = 300$ Pa, $\mu = 300$ Pa s. The data for tractoring force-velocity and the linear relationship predicted by equation 4.6 are shown in figure 4-14 . At the given interwave velocity $\hat{V}_i = 0.5$ cm/s and fluid properties, the snail generated a high amount of wave drag, such that even at zero tractoring force,

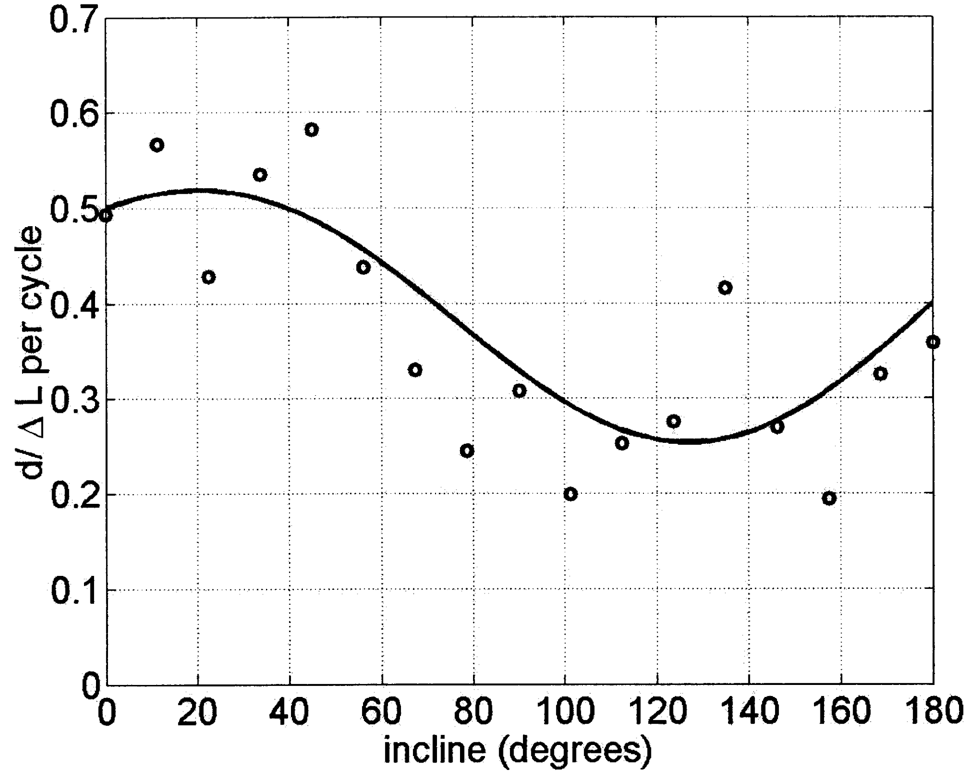

Figure 4-13: Displacement per cycle of Robosnail 2a, on Laponite solution, 7.5 % by weight. The snail functioned the best on the horizontal, where gravity was not pulling against the direction of motion or away from the substrate. The worst performance occurred at 90 degrees vertical incline, when the snail had the greatest force resisting its motion.

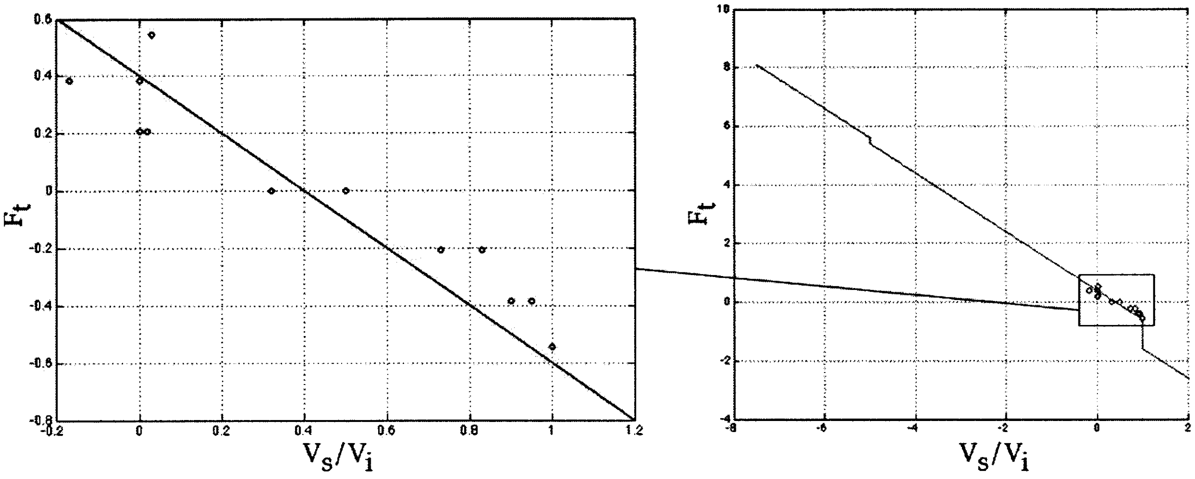

Figure 4-14: Robosnail 2 tractoring force vs. normalized tractoring velocity. The working fluid is a Carbopol solution, 7% by weight. The measurements show good agreement with the tractoring force-velocity relationship derived earlier (equation 4.6) for a Bingham fluid with τ_y = 300 Pa, μ = 300 Pa s. The mass of the snail was 300 g, while the interwave velocity was 5 mm/s. The resultant Bingham number for these parameters is $B = 0.6$.

there was a finite amount of back-slip. Only when given a positive tractoring force did the snail travel at the no-slip velocity $\hat{V}_i$.

Because of the higher yield stress of the Carbopol solution compared to the Laponite solution, the heavier snail could be supported on a vertical surface. While both models could be supported for up to sixty seconds upside-down, eventually the foot would delaminate from the substrate and the snail would fall away. The delamination was most likely caused by the open construction of the segmented foot; as the segments slid over the layer of lubricating fluid, they entrained air bubbles which slowly grew in size, and eventually contributed to large-scale separation between the foot and the fluid. Live snails do not have this problem, as they have a continuous foot with a smaller perimeter that can prevent undesirable leakage of air, and they are able to sense and adjust to momentary separations from the substrate.

Chapter 5

Three-Link Swimmer

5.1 Introduction

The Three-link swimmer was inspired by E.M. Purcell's talk "Life at Low Reynolds Number" [41]:

> "There is a very funny thing about motion at low Reynolds number, which is the following. ...if (an) animal tries to swim by a reciprocal motion, it can't go anywhere. Fast or slow, it exactly retraces its trajectory and it's back where it started. ... The moral of this is that the scallop at low Reynolds number is no good. ...The simplest animal that can swim that way is an animal with two hinges. I don't know whether one exists ..."

In his talk, Purcell describes the realm of the low Reynolds numbers, where the effects of viscosity dominate, and momentum effects are negligible. Most swimming and flying organisms and devices familiar to man (e.g. birds, fish, airplanes) operate at high Reynolds number, where propulsive forces are generated by momentum transfer. Because of the paradigm shift from inertia-based to drag-based propulsion, many of the locomotion methods that are effective at low-Re are counterintuitive, and many high-Re locomotion methods are useless at low-Re [47].

Figure 5-1 illustrates the motion of the swimmer described by Purcell. During one cycle of motion, the swimmer executes four similar strokes. Because each of the fins flaps independently and out-of-synch with the other flap, the motion is not reciprocal.

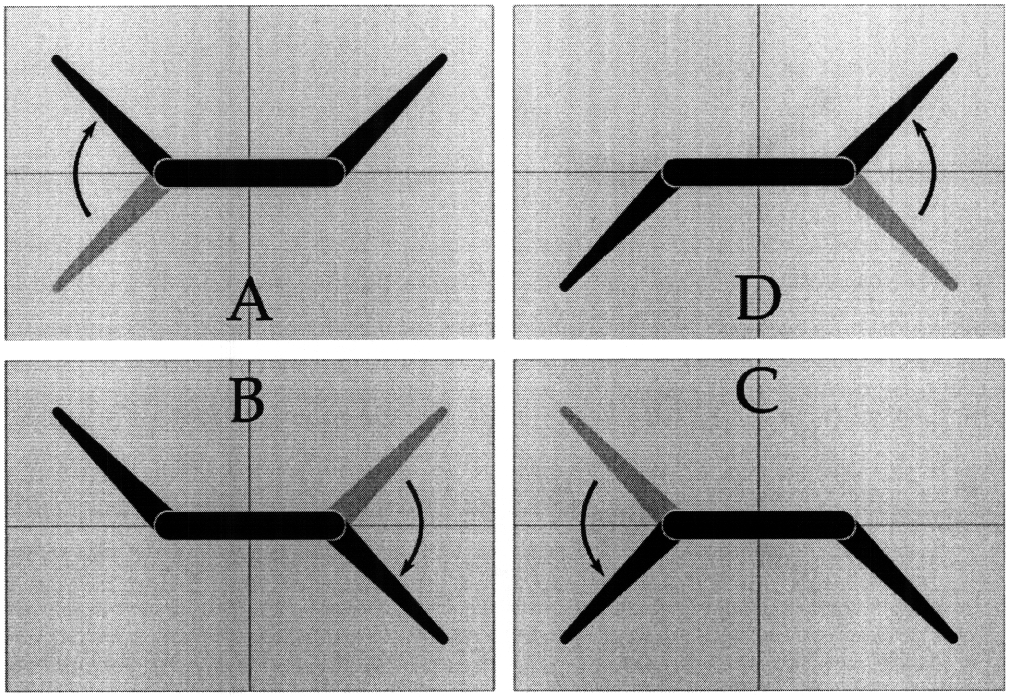

Figure 5-1: Motion sequence of three-link swimmer.

5.2 Theory

In the limit of low Reynolds number (the Stokes limit), the Navier-Stokes equations reduce to the Stokes equations, which are time-independent [41, 12]. Because of the resulting reversibility, reciprocal motions generate no net displacement.

A two-link swimmer such as a simplified scallop, for example, is only capable of opening and closing. Whatever net motion experienced by the scallop in its opening stroke would be cancelled exactly during the closing stroke. Likewise, the rightward tail swing of a fishlike swimmer would cancel the effect of a leftward swing of its tail. Flapping a pair of wings, one of the most efficient methods of high-Re propulsion, becomes useless in the Stokes limit. Because of the constraint of reversibility, three is the minimal number of oscillating links required to compose a successful swimmer. (For non-reciprocating joints, two can suffice: as in the helical flagella swimmers, constant forward rotation in one direction comprises non-reciprocal motion. The bacterium *E. coli* is an example of a helical flagella swimmer.).

The optimality of swimmers of various geometries has been considered analytically [5], and numerical studies of a thin body version of the three-link swimmer (a swimmer composed of three thin, rigid cylinders) [8, 46] have been done. Because of the complexity of the

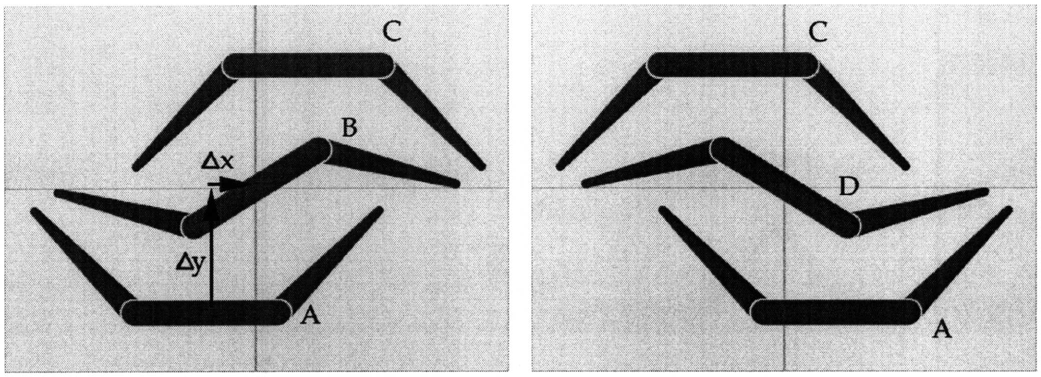

Figure 5-2: Hypothetical motion of the three link swimmer. The swimmer starts at "A", and flaps its right-side fin downward, moving the swimmer some x and y displacement Δx, Δy. From reversibility, this is the same as the reverse motion from B to C, and the sequence from C back to A is the same as the time-reverse mirror image from A to C. Thus we only need to know the motion from A to B to understand the full cycle.

flow around a swimmer composed of flat plates, we experimentally optimize the geometry of the swimmer, by varying fin length with relation to the body.

The symmetry of the theoretical swimmer and its stroke pattern greatly simplify the analysis of the swimmer. In fact, one needs only analyze the motion of a single sweep of one arm to understand the entire motion of the swimmer, and one can conclude that the swimmer must move in a straight line (Figure 5-2). This simplification is a result of two symmetries of the motion cycle: the flap of one fin is identical to the time-reverse flap of the second fin, while mirroring these two motions results in the third and fourth steps in the cycle.

There is also the question of the effect of increasing the size of the flapping fins in relation to the body. When normalized to the full body length (both fins plus mid-section), the limiting cases for fin length are zero length (an immobile body) or half the body length (no body, just fins, resulting in a two-link swimmer or scallop). As either of these cases results in zero displacement, there must be some optimal arm length a that maximizes the speed of the swimmer. Likewise, the angle of the stroke can also be optimized. It was found by Tam [46] that the best stroke (for the planar swimmer composed of filaments) involves constant variation of both joints rather than discrete motion of one after the other, and that there exist separate optimizations for either maximizing the energy efficiency, or the displacement per cycle.

5.3 Mechanical Design

The three-link swimmer was built to have three panel-like linkages, as opposed to long, narrow linkages as described in Purcell's talk and the literature. This was a practical compromise as the difficulties of placing the driving mechanism and power source in a narrow linkage would increase to the point of impracticality for a device that was to be small enough to operate at low Reynolds number.

The swimmer is powered by a clock spring, which led to a simpler design (compared to a motorized swimmer), and added the benefit of making the actuation mechanism smaller and less negatively buoyant compared to a motor-battery-gearbox assembly.

The spring generated a rotary motion, which needs to be translated to the flapping of both end links (fins). To actuate the flapping of the fins, we mounted the spring on its inner end and attached the free end to a rotating ring. The outer edge of the ring was shaped to have sloped sections in contact with part of the moving links/fins. As the ring rotated, the sloped edge would flip the fins to the left and right, causing the flapping motion. An important feature as discussed earlier was for the movement of one fin to alternate with the motion of the other. This is solved by placing the rotating axis of the ring to be offset from the imaginary line connecting the contact points of the fin.

All of the parts, with the exception of the spring and some small fasteners, were machined from polycarbonate and delrin plastics to keep the buoyancy to be as close as possible to neutral with respect to the working fluids, glycerol and silicone oil. A small foam float was added to keep the device from sinking.

5.4 Experiment

As the only requirement for the operating fluid was that it be Newtonian and of a significant viscosity, there were several choices. For practical reasons, we chose silicone oil, as opposed to water soluble fluids, which would eventually corrode the steel clock-spring. The mechanical swimmer was operated with clear fluid to first test that there was positive travel. Later we put neutrally buoyant tracer particles and dye into the fluid to trace the fluid motion.

Another test would be to increase or decrease the arm lengths in relation to the body length and to experimentally find an optimal length to maximize the displacement per cycle.

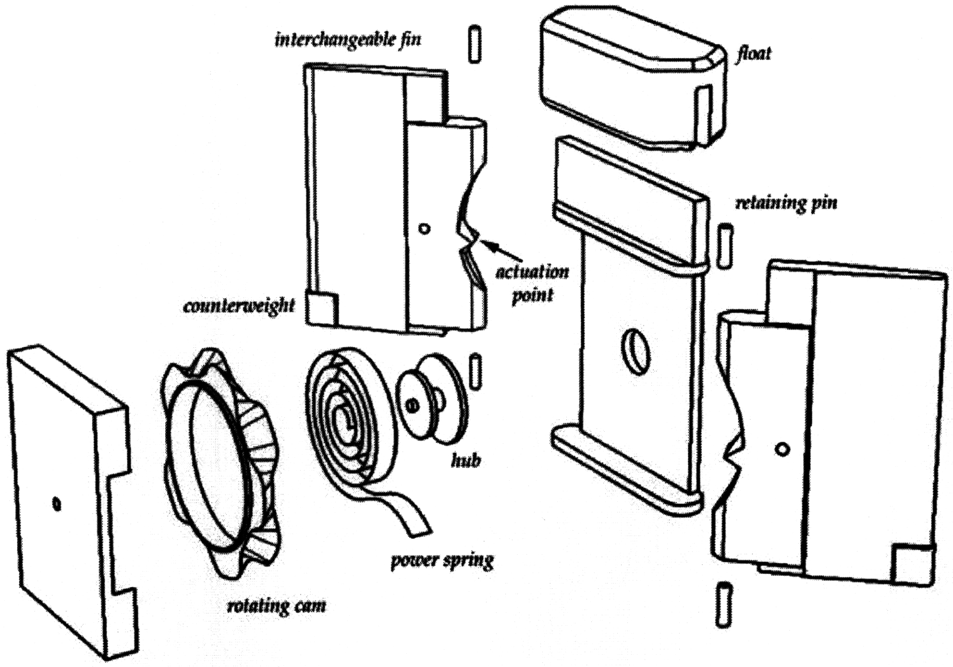
interchangeable fin
float
retaining pin
actuation point
counterweight
hub
power spring
rotating cam

Figure 5-3: Exploded view of three-link swimmer

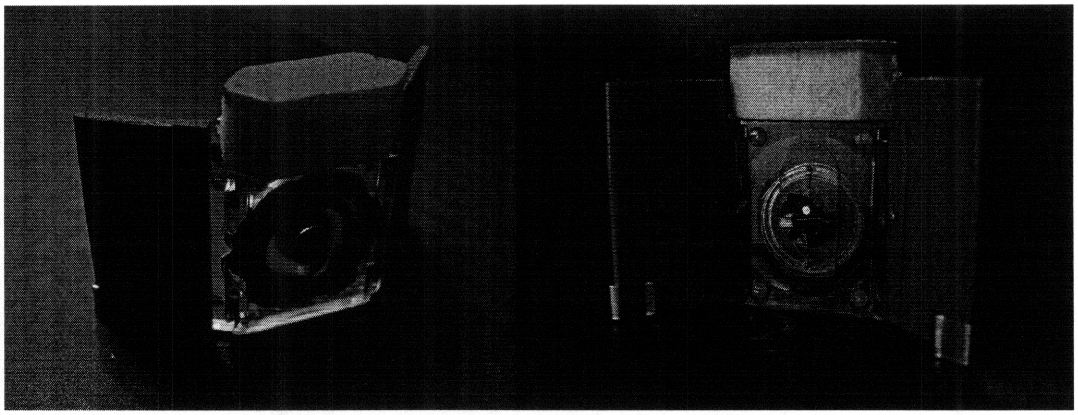

Figure 5-4: The three-link swimmer.

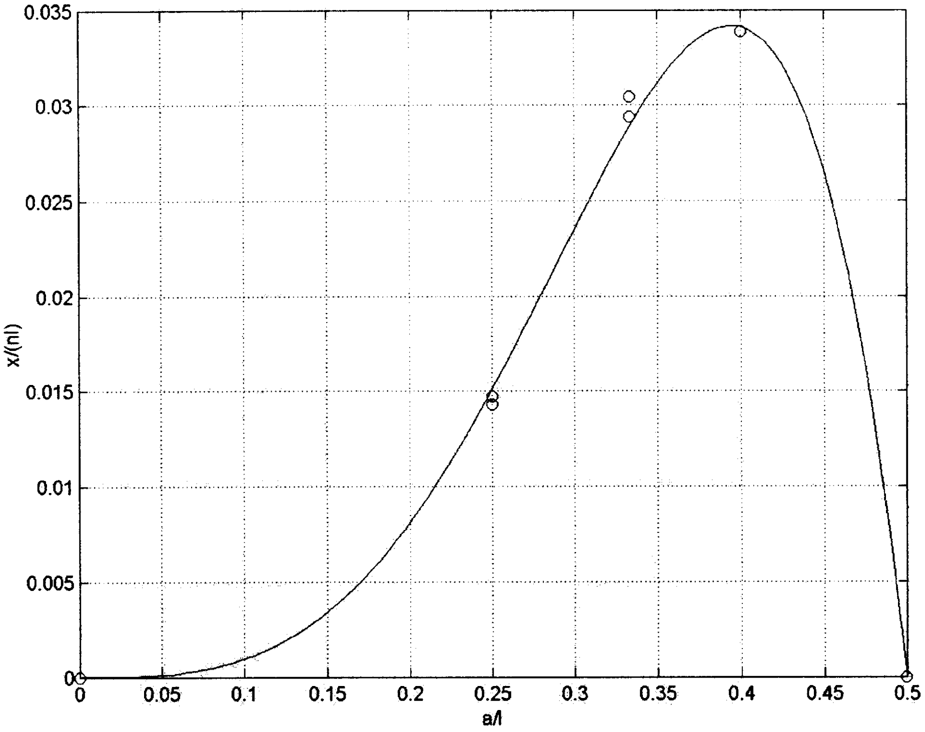

Figure 5-5: Distance traveled for the three-link swimmer, normalized to total unfolded body length, as a function of the fin/arm lengths. (The curve shown is a best-fit polynomial is to guide the eye and not directly related to the theory.)

5.5 Results and Discussion

First, the mechanical three-link swimmer successfully propelled itself through a high viscosity Newtonian fluid at a rate of several percentages of the body length per cycle. The displacement per cycle was shown to vary when the lengths of the arms were changed. Two arm-lengths besides 1:1 were tried and the displacements were normalized to the total swimmer length.

The experimental results seem to suggest an optimum arm size around b = 0.4, resulting in the maximum measured swimmer velocity near 0.034 body lengths per cycle. The flow around the three-link swimmer was fully 3D, and unlike the Becker swimmer, could not be analyzed with the theory of thin bodies. However, the real swimmer experiment provided us with qualitative information on the fluid dynamics of its swimming action. Like Becker [8], Tam [46] conducted extensive numerical studies in the search for an optimized swimming stroke and swimmer shape of a 3-link swimmer (Tam extends the analysis to compare optimal n-link swimmers and swimmers with a body). As the findings of Tam and Becker suggest, the optimal fin length is roughly equal to the mid-segment length, which is consistent with our prototype swimmer results.

Neutrally buoyant tracer particles (Kalliroscope ® rheoscopic fluid in some tests, and small plastic beads in other runs) were planted in the fluid to trace the fluid motion as the swimmer propelled itself past. This low-tech flow visualization method allowed us to understand better the fluid dynamics of the swimmer.

Like any self propelling body, the swimmer generates a thrust wake, pushing fluid backwards as it moves forward. There is however a large region of fluid being pulled along with the swimmer, as the no-slip condition is significant at extremely low Reynolds numbers. Lastly, because the fluid is incompressible, the fluid is pulled in from the sides to make up for the fluid moving to the fore and aft of the swimmer. Even after five cycles, these flow characteristics are clearly visible in the tracer lines.

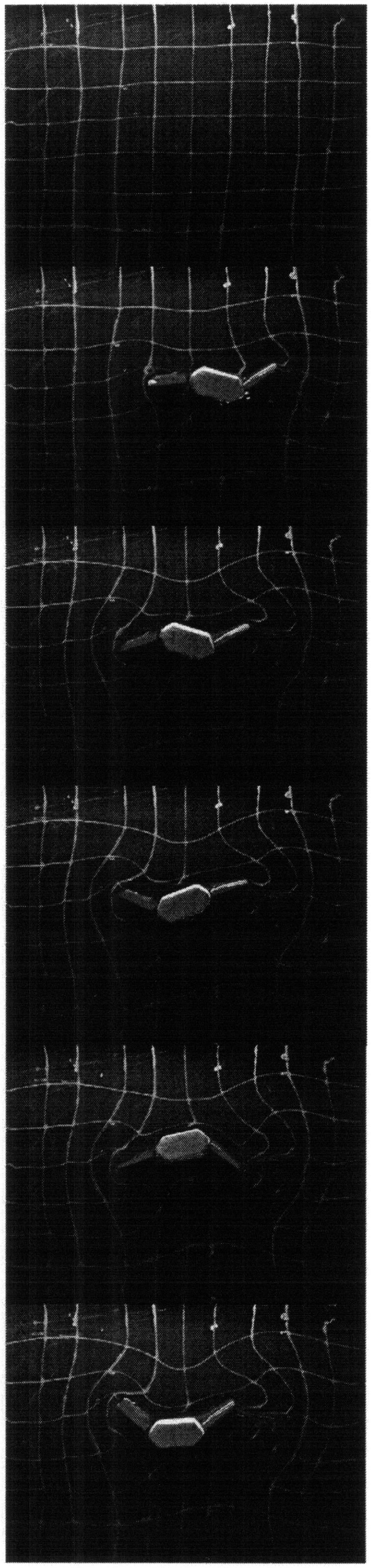

Figure 5-6: The three-link swimming next to fluid tracers. As the swimmer moves, it drags a portion of the fluid along with itself in the direction of motion, according to the no-slip condition, while simultaneously sending fluid backward in order to propel itself forward. As a result of fluid being forced forward and backward, the fluid is pulled in from either side of the swimmer, contracting lengthwise gridlines.

Chapter 6

Applications

6.1 General Applications

Robosnail 1 and Robosnail 2 type robots may find use in a variety of applications that require locomotion or the application of force, where high speeds are not essential. At low Reynolds numbers a Robosnail-1 type robot would be effective in moving itself or other objects in the presence of a thin layer of fluid. Small-scale robots for navigating the human body would likely be traveling at low Re due to their small size and low speeds. In many cases, they may come into contact with, or be completely immersed in non-Newtonian fluids.

6.2 Downhole locomotion

In the oil drilling industry, it is sometimes necessary to send sensing robots into the ground to gather data from a potential drilling site. The holes drilled for data collection and subsequent oil extraction (downholes) are typically pressurized and filled with natural or synthetic muds. It can be difficult to send robots into the drilled holes, as the presence of mud often limits traction, creating a lubrication layer that allows conventional gripping surfaces to slip on the substrate. A snail-like device, however, would be able to exploit the viscous and/or non-Newtonian properties of mud to move through such difficult terrains. A robosnail 1 device is being patented [9] for this application.

6.3 Rigless tool Deployment

In addition to sending powered tools and logging equipment into downholes, another application would be to use a stationary device to push measurement tools into the downhole. These devices must be capable of sustaining extremely high forces to counteract the extreme pressure of the fluids within the downhole. Current technologies involve gripping tools with solid grippers, which risks damaging the surface of the tools from the stress concentrations at the gripping point. A sliding gripper with a design based on that of Robosnail 2, given the correct yield-stress fluid, would be able to continuously support a tool.

6.4 Flexible robotics

The interest in snails and snail locomotion has inspired a new type of flexible robot dubbed the "Squishbot". As its name implies, the Squishbot is designed to radically change its size and shape in order to navigate tight places and squeeze through narrow constrictions. Robosnail 2 was designed with soft actuators in mind; as these become more efficient and effective, the next step is to incorporate soft actuators as muscles to replace the rigid transmission system of robosnail 2. In this sense it would approach the simplicity of design and versatility of its natural counterpart.

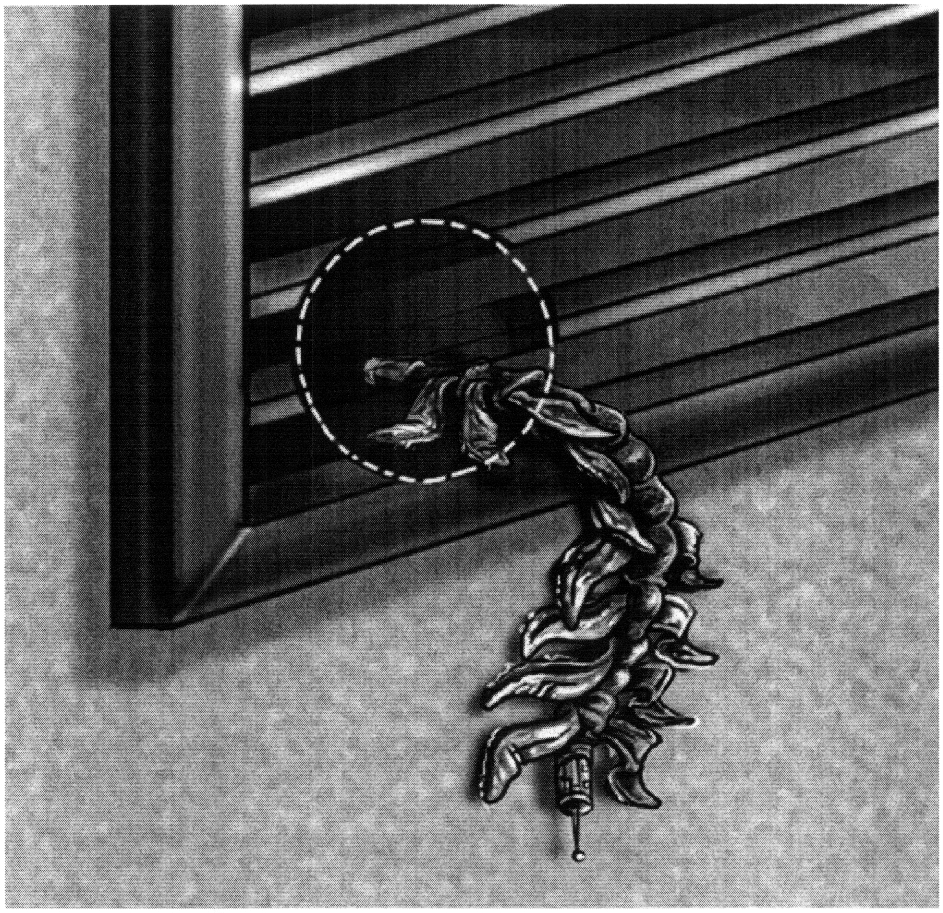

Figure 6-1: “Squishbot”, a proposed flexible robot capable of changing size and shape. Such a robot will use flexible actuators and apply a method of locomotion similar to robosnail 2. Squishbot a joint project between MIT and Boston Dynamics, and is funded by the Defense Sciences Office at DARPA as part of the Chembots program. Artwork is from Boston Dynamics [2]

Chapter 7

Conclusion

We have introduced three novel methods of locomotion through viscous Newtonian and non-Newtonian fluids. Research on Robosnail 1 has shown that peristaltic waves of a membrane can generate significant propulsive forces when lubricated with a Newtonian fluid and brought close to a solid substrate. The theory and numerical simulations reveal the various characteristic forces and velocities that can be attained by changing the waving profile, and experimental results confirm the results for the basic, sinusoidal wave shape. The numerical simulations also showed the relative effect of leakage flows when the width of the snail was finite.

Robosnail 2 exploited the non-Newtonian properties of shear-thinning fluids to move in a way analogous to live snails, which use shear - thinning mucus to propel themselves. Like its live counterparts, robosnail 2 was able to climb walls and ceilings. We have formed a general theory to relate the velocity and force to the snail geometry, as well as a more specific theory to describe the motion in the special case where the lubricating fluid is a Bingham fluid. Experiments using aqueous suspensions of Carbopol and Laponite, synthetic shear-thinning fluids, led to successful tests of locomotion on a range of inclines from 0 to 180 degrees.

The three-link swimmer was shown to propel itself successfully as Purcell predicted. It was found that the swimming velocity was greatest when the fins were the same length as the body, this being the expectation as much smaller or much larger fins would be closer to the limiting cases where displacement is known to be zero. Flow visualization experiments illuminated the process by which the fluid is displaced as the swimmer moves. The optimum fin size for maximizing distance traveled per cycle was found experimentally.

7.1 Future work

The three-link swimmer was built as a proof-of-concept. While it functioned as we expected, it did not consist of a geometry as mathematically simple as the thin forms studied by Becker and Tam. The shape consisting of flattened panels was adopted as a matter of practicality. Future generations of the three-link swimmer should incorporate thin filamentous sections; we would expect the experimental results to closely match the theoretical results of Becker and Tam. In addition to three-link swimmer, Tam wrote numerical simulations of n-link swimmers, and found optimal swimming patterns for such multi-link devices. Experimental verification of these as well as other swimming methods would be important in the quest to build better low-Re devices. Furthermore, the Tam swimmer varied from the prototype three-link swimmer in that not only was the optimal geometry studied, but the stroke cycle. Tam et al. found that the stroke pattern could be further optimized by incorporating overlapping strokes between the two fins; for the most efficient swimmer, one fin would still be moving when the second fin begins to flap. Experimental verification of the phase overlap optimization has not yet been done but could be achieved with a more sophisticated actuation mechanism.

This research was carried out with the intention to determine the feasibility of new types of locomotion in fluid. While each of the devices was capable of locomotion in a manner consistent by the theory, they were rigid and designed to move in a straight line. The next obvious step would be to add control and steering. In the case of the snail, the goal would also include taking full advantage of a live snail's flexibility by incorporating a soft foot. The snail-like devices shown here were limited also by the fact that they did not carry their own mucus supply, unlike real snails. Future generations should be completely self-contained in this respect. It was found that a robosnail 1 employing various wave profiles could be optimized for various situations. It would be useful to design and test prototype snails that used these non-sinusoidal wave profiles.

Two of the three mechanisms presented here have been actuated using rotational actuators, but could be simplified with the use of linear actuators. The use of soft, muscle-like linear actuators would result in a robot very much like the invertebrate on which it is based.

A robosnail 2 using a soft foot would be more effective at conforming to irregular terrains. The evolution of these devices along with new innovations in soft actuators may lead to machines with functionalities that match or surpass that of natural organisms.

Bibliography

[1] Laponite- synthetic layered silicate- its chemistry, structure, and relationship to natural clays. Technical report, Rockwood Additives Limited, Moorfield Road, Widnes, Cheshire WA8 0JU, UK.

[2] "Boston Dynamics". http://bostondynamics.com/robot_squishbot.html, 2009.

[3] B. Abou, D. Bonn, and J. Meunier. "Nonlinear rheology of Laponite suspensions under an external drive". *J.Rheol*, 47:979, 2003.

[4] A. Ajdari and H.A. Stone. "A note on swimming using internally generated traveling waves". *Physics of Fluids*, 11:1275–1277, 1999.

[5] J. Ashmore, C. del Pino, and T. Mullin. "Cavitation in a lubrication flow between a moving sphere and a boundary". *Phys. Rev. Lett.*, 94:124501, 2004.

[6] J. Avron and O. Kenneth. "Optimal Swimming at Low Reynolds Numbers". *Phys. Rev. Lett.*, 93:186001, 2004.

[7] N.J. Balmforth and R.V. Craster. "A consistent thin-layer theory for Bingham Plastics". *J. Non-Newtonian Fluid Mech.*, 84:65, 1999.

[8] L.E. Becker, S.A. Koehler, and H.A. Stone. "On Self-Propulsion of Micro-Machines at Low Reynolds Number: Purcell's Three-Link Swimmer". *Journal of Fluid Mechanics*, 490:15–35, 2003.

[9] B. Chan. Mechanical crawler. Patent Pending, Oct 2005. US 2007/0079997 A1.

[10] B. Chan, N.J. Balmforth, and A.E. Hosoi. "Building a better snail: Lubrication and adhesive locomotion". *Physics of fluids*, 17:113101, 2005.

[11] B. Chan, S. Ji, C. Koveal, and A.E. Hosoi. "Mechanical Devices for Snail-like Locomotion". *Journal of Intelligent Material Systems and Structures*, 18:111–116, 2007.

[12] S. Childress. *The Mechanics of Swimming and Flying.* Cambridge University Press, Cambridge, 1997.

[13] R.B. Clark. *The Dynamics of Metazoan Evolution.* Clarendon Press, Oxford, 1964.

[14] R.B. Clark and J.B. Cowey. "Factors controlling the change of shape of certain nemertean and turbellarian worms". *J. Exp. Biol.*, 35:731, 1958.

[15] M. Denny. "The role of gastropod pedal mucus in locomotion". *Nature*, 285:160–161, 1980.

[16] M. Denny. "A quantitative model for the adhesive locomotion of the terrestrial slug, *Ariolimax columbianus*". *Journal of Experimental Biology*, 91:195–217, 1981.

[17] M. Denny. "Mechanical properties of pedal mucus and their consequences for gastropod structure and performance". *American Zoology*, 24:23–36, 1984.

[18] M. Denny. "Invertebrate mucous secretions: functional alternatives to vertebrate paradigms". *Symp. Soc. Exp. Biol.*, 43:337–366, 1989.

[19] W.R. DiLuzio, L. Turner, M. Mayer, P. Garstecki, D.B. Weibel, H.C. Berg, and G.M. Whitesides. " *Escherichia coli* swim on the right-hand side". *Nature*, 435:1271–1274, 2005.

[20] H.Y. Elder. "Direct peristaltic progression and the functional significance of the dermal connective tissues during burrowing in the polychaete *Polyphysia crassa* (Oersted)". *J. Exp. Biol.*, 58:637, 1973.

[21] R. Ewoldt. *Nonlinear viscoelastic materials: new characterization measures and bioinspired applications.* PhD thesis, Massachusetts Institute of Technology, May 2009.

[22] R. Ewoldt, C. Clasen, A.E. Hosoi, and G. McKinley. "Rheological fingerprinting of gastropod pedal mucus and synthetic complex fluids for biomimicking adhesive locomotion". *Soft Matter*, 3:634–643, 2007.

[23] B.U. Felderhof. The swimming of animalcules. *Phys. Fluids*, 18:063101, 2009.

[24] J. Gray. *Animal Locomotion.* Weidenfeld and Nicolson, London, 1968.

[25] Jones. H.D. *Locomotion. In* Pulmonate molluscs. Cambridge University Press, London and New York, 1974.

[26] A. Ito and H. Yasukawa. "Film structured soft actuator for biomimetics of snail's gastropod locomotion". *The 6th International Converence on Control, Automation, Robotics and Vision ICARCV*, 2000.

[27] H.D. Jones. "The Mechanism of locomotion of *Agriolimax reticulatus* (Mollusca: Gastropoda". *J. Zool. Lond.*, 171:489, 1973.

[28] H.D. Jones and E.R. Trueman. "Locomotion of the impet, *Patella vulgata*". *Journal of Experimental Biology*, 52:201, 1970.

[29] E. Lauga, W.R. DiLuzio, G. Whitesides, and H.A. Stone. "Swimming in circles: motion of bacteria near solid boundaries". *Biophys. J.*, 2006.

[30] J. Lighthill. "Flagellar Hydrodynamics". *SIAM Review*, 18:161, 1976.

[31] H.W. Lissman. "The mechanism of locomotion in gastropod molluscs, I. Kinematics". *Journal of Experimental Biology*, 21:58, 1945.

[32] H.W. Lissman. "The mechanism of locomotion in gastropod molluscs, II. Kinetics". *Journal of Experimental Biology*, 22:37, 1946.

[33] L. Mahadevan, S. Daniel, and M.K. Chaudhury. "Biomimetic ratcheting motion of a soft, slender, sessile gel". *Proc. Natl. Acad. Sci USA*, 101:23, 2004.

[34] C. Mettam. "Segmental musculature and parapodial movement of *Nereis diveriscolor* and *Nephtys hombergi* (Annelida: Polychaeta)". *J. Zool., Lond.*, 163:489, 1961.

[35] S. Moffett. "Locomotion in the primitive pulmonate snail *Melampus bidentatus*: Foot structure and function". *Biol. Bull.*, 157:306, 1979.

[36] J. Moore. *An Introduction to the Invertebrates.* Cambridge University Press, Cambridge, 2001.

[37] Q.D. N'guyen and D. V. Boger. "Measuring the flow properties of yield-stress fluids". *Ann. Rev. Fluid Mech.*, 24:47–88, 1992.

[38] J.G. Oldroyd. "Two-dimensional plastic flow of a Bingham solid: a plastic boundary-layer theory for slow motion". *Proc. Camb. Phil. Soc.*, 43:383–395, 1947.

[39] C.F.A. Pantin. "Locomotion of nemertines". *Proc. Linn. Soc. Lond. (Zool.)*, 162:23, 1950.

[40] R. Pearl. "The movements and reactions of freshwater planarians: a study in animal behavior". *Quart. J. micr. Sci.*, 46:509, 1903.

[41] E.M. Purcell. "Life at Low Reynolds Number". *American Journal of Physics*, 45:3–11, 1977.

[42] O. Reynolds. "On the theory of lubrication and its applications to Mr. Beauchamp Tower's experiments, including an experimental determination of the viscosity of olive oil". *Philos. Trans. R. Soc. London*, 177:157, 1886.

[43] EE Ruppert and R.D. Barnes. *Invertebrate Zoology.* Harcourt Brace College Publishers, New York, 1994.

[44] A. Shapere and F. Wilczek. "Self-Propulsion at Low Reynolds Number". *Phys. Rev. Lett*, 58:2051, 1987.

[45] DD Spain and WM Kier. "Peristaltic locomotion in holothuroids (Echinodermata)". *Integr. Comp. Biol*, 42:1316–1316, 2002.

[46] D. Tam and A.E. Hosoi. "Optimal Stroke Patterns for Purcells Three-Link Swimmer". *Physical Review Letters*, 98:068105, 2007.

[47] G.I. Taylor. "Analysis of the swimming of microscopic organisms". *Proceedings of the Royal Society of London, Ser. A*, 209:447, 1951.

[48] E.R. Trueman. "The fluid dynamics of molluscan locomotion". *Malacologia*, 9:701, 1969.

[49] E.R. Trueman. *The Locomotion of Soft-Bodied Animals.* American Elsevier Publishing Company, New York, 1975.

[50] F Vlès. "Sur les ondes pediuses de Mollosques reptateurs". *C. R. Hebd. Seances Acad. Sci.*, 145:276, 1907.

[51] J. Wikening. Convergence of reynolds' lubrication approximation and its higher order corrections on a periodic domain. Technical Report LBNL-61019, Lawrence Berkeley National Laboratory, 2006.

[52] J. Wilkening and A.E. Hosoi. "Shape optimization of a sheet swimming over a thin liquid layer". *J. Fluid Mech.*, 601:25–61, 2008.

[53] N Willenbacher. "Unusual Thixotropic Properties of Aqueous Dispersons of Laponite RD". *Journal of Colloid and Interface Science*, 182:501–510, 1996.